Optimisation of the Pulse-Echo Method with an Application to Acoustic Thermometry

G.C. Burger

Supervisor: Mr B. Groenewald
Co-supervisors: Dr J. Davies & Prof G. De Jager
Centre for Instrumentation Research

Submitted in fulfillment of the
requirements for the
degree of Magister Technologiae
in the Department of Electrical Engineering

Cape Peninsula University of Technology
Cape Town

March 2010

Declaration

I, Gert Cloete Burger, declare that the contents of this thesis represent my own unaided work, unless stated otherwise, and that the thesis has not previously been submitted for academic examination toward any qualification. Furthermore, it represents my own opinions and not necessarily those of the Cape Peninsula University of Technology.

Signature of author ....

Cape Town

Declaration

I, Gert Cloete Burger, declare that the contents of this thesis represent my own unaided work, unless stated otherwise, and that the thesis has not previously been submitted for academic examination toward any qualification. Furthermore, it represents my own opinions and not necessarily those of the Cape Peninsula University of Technology.

Signature of author ....

Cape Town

Acknowledgments

I would like to acknowledge and extend my heartfelt gratitude to the following persons for making the completion of this thesis possible:

- My supervisors, Mr B. Groenewald, Dr J. Davies and Prof G. De Jager, thank you for your patience, guidance and support;

- fellow students and staff at the Centre for Instrumentation Research at the Cape Peninsula University of Technology;

- everyone at Radical Electronic Systems for their assistance;

- Mr D. De Villiers, for your advice and friendship;

- Miss L. Koch, for your love and support;

- most especially, to my mother, father and brothers, thank you for your patience, support and love.

Abstract

In acoustics, pulse echo methods are well known as a means of measuring time of flight. Traditional techniques for generating acoustic waves in solid ferromagnetic waveguides include piezoelectric, capacitive and magnetostriction. Piezoelectric and capacitive techniques are preferred due to the inefficiency of magnetostriction caused by electro-mechanical coupling losses and the fact that most ferromagnetic materials show low levels of magnetostriction. The aim of this study was to optimise the magnetostrictive effects for sensing applications based on a ferromagnetic waveguide using the pulse echo method. The results obtained were implemented in the design of an acoustic thermometer.

Two configurations for signal generation and recovery were examined, the use of a single wound copper coil acting as a transceiver coil, and the use of separate transmit and receive coils. Results obtained using the latter configuration indicated better signal to noise ratio's and provided the flexibility to manipulate the point of signal recovery. The pulse echo method was implemented and optimised.

An acoustic thermometer based on an existing design was developed by inducing a partial reflection from a set position in the waveguide, defining a sensing probe. Awareness of the elastic properties of the waveguide material enabled the guaging of its temperature by measuring the acoustic pulse velocity in the probe.

The accuracy of the instrument was increased through signal conditioning, examined together with cross correlation and an increased sampling frequency. Systematic errors were resolved through calibration, giving the instrument an overall accuracy of $\pm 0.56^{\circ}C$ for the range of temperatures between $20^{\circ}C$ and $400^{\circ}C$.

Contents

List of Figures

vii

List of Tables

Nomenclature

α	Constant of proportionality
Λ	Magnetostrictive stress constant
μ_0	The permeability of free space
μ_r	Relative permeability
ω	Angular velocity
Φ	Magnetic flux
ρ	Density
σ	Applied stress
ξ	Strain
A	Area
B	Magnetic induction
c	Velocity of sound
D	Distance
F	Force
H	Magnetic field strength
l	Length
M	Magnetisation
N	Number of turns
SD	Standard deviation
u	Particle velocity
Y_0	Young's modulus
Z	Impedance

Chapter 1

Introduction

1.1 Background

Ferromagnetic materials have the property that when placed within a magnetic field they are mechanically deformed. This phenomenon was first discovered by James Prescot Joule in 1847, when he positively identified the change in length of an iron sample as its magnetisation changed. This is known as the Joule or magnetostrictive effect. Villari discovered in 1864 that when mechanical stress is placed on ferromagnetic materials, its magnetic induction changes, thus proving the inverse magnetostrictive effect [Kwun & Bartels, 1998].

The magnetostrictive effect is used to launch a longitudinal strain pulse into a waveguide made of ferromagnetic material. This strain pulse propagates along the axis of the waveguide at the velocity of sound for that specific material. The inverse of the magnetostrictive effect is used to recover the echoes of the launched pulse. As the ferromagnetic waveguide is affected by external parameters such as temperature, stress and magnetic fields, its physical properties will change. These changes are reflected in the recovered signal echoes.

Implementing ferromagnetic waveguides as magnetostrictive delay lines have been done for a wide range of sensing applications, including position or distance sensors [Karagiannis *et al.*, 2003], longitudinal or torsional stress sensors [Lynnworth, 1977], liquid level and viscosity sensors [Kim & Bau, 1989b] [Kim & Bau, 1989a] [Glover *et al.*, 1968] and temperature sensors [Fathimani & Bell, 1978] [Bell, 1972] [Tasman & Patzold, 1980] [Bell & Mosby, 1970] [Lynnworth *et al.*, 1965]. The latter is more commonly referred to as acoustic thermometers.

1.2 The Pulse Echo Method

The pulse echo method is achieved by launching an acoustic pulse into a specific media and recovering the resultant echo signals. The properties of the media through which the acoustic wave propagated could be established by investigating the characteristics of the recovered echo

1

signal. These characteristics include the amount of attenuation suffered, the time delay between returning echoes and the shape of the recovered echo signal.

The attenuation suffered by acoustic pulses propagating in solid media is high, largely due to internal friction [Coulter, 1987]. This stipulates the importance of efficient wave generation and recovery. In order to achieve higher resolutions from an acoustic sensor, the magnitude of the launched acoustic pulse in the media had to be maximised, along with optimal recovery of the launched acoustic pulse.

1.2.1 Acoustic Thermometry

Magnetostrictive waveguides implemented as temperature sensors employ one of two basic methods of functionality. The pulse echo method or the resonance method [Lynnworth, 1975]. These methods depend on the temperature dependence of the elastic properties of the waveguide material, more specifically the velocity of sound, c, in the material.

The resonance method is set up using a magnetostrictive waveguide terminated in a resonator section which constitutes the sensing probe. A pulse train signal is then transmitted through the waveguide to the probe section at the resonant frequency of the sensing probe. The resultant echo signal is then observed as the decrement of the echo indicates whether the probe section is at resonance. The resonance frequency of the probe material changes because the density and elasticity of the material changes with temperature. The resonant frequency of the probe can be directly related to the temperature of the probe if the elastic properties of the probe material as a function of temperature is known. The material used for and the shape of the resonator determines the range and accuracy of the sensor. These aspects were investigated by Fathimani & Bell [1978] and optimal results found using a tuning fork shaped probe. Sapphire and tungsten was specified as materials used for the probe section and their resonant acoustic thermometer had an accuracy of $\pm 2^{\circ}C$ over the range of temperatures up to $2000^{\circ}C$.

The pulse echo method is less complex to implement than the resonance method. The pulse echo method for acoustic thermometry is implemented by measuring the velocity of an acoustic pulse propagating through a defined section of the waveguide. The temperature of the defined section of the waveguide can then be established if the elastic properties of the waveguide material is known. The pulse echo method relies on the reflections of acoustic pulses from set boundary conditions along the path of propagation. Nominally, the time delay is measured between two acoustic reflections, originating from the beginning and the end of the defined probe section. This makes it possible to measure the temperature of multiple sections along a single waveguide [Lynnworth, 1970] [Lynnworth & Spencer, 1970] [Varela, 1984]. Mi *et al.* [2003] specifies from results obtained a time resolution of $0.2\mu s$ in the measurement of the time delay between reflections. An accuracy of 0.033% in the measurement of a time delay of $100\mu s$ is specified by Bell [1957].

2

1.3 Objectives

The objective of this research was to optimise the pulse echo method for sensing applications, based on a ferromagnetic waveguide and using magnetostriction for signal generation and recovery. A thorough investigation into the factors that affected the effective launch and recovery of acoustic pulses in a ferromagnetic waveguide had to be completed. A study of the behavior of the propagating acoustic pulses in the waveguide was necessary. The necessary hardware had to be designed to complete the investigation. The optimised acoustic waveguide setup had to be quantified for implementation as a sensing solution, more specifically an acoustic thermometer.

The knowledge gained through the investigation and optimisation of the pulse echo method and a ferromagnetic waveguide had to be consolidated in the design of an acoustic thermometer. The resolution of the acoustic thermometer had to be comparable to that of previous researchers. The effect that the addition of powerful data acquisition hardware and the signal processing method cross correlation had on the resolution of the designed thermometer had to be investigated. Finally, the accuracy of the designed instrument had to be established and the results concluded.

1.4 Delineation

The generation and recovery of longitudinal strain pulses using the effects of magnetostriction will be investigated. The magnetostrictive effects will be generated with the use of wound copper coils. The use of other pulse generation methods, such as piezo-electric transduction, will not be investigated. The ferromagnetic material nickel will be used as waveguide material and other materials such as cobalt and terfenol-D will not be investigated. Reflection of the signal echoes from the ends of the waveguide and effective termination will be investigated.

The frequency range of the launch pulse to be investigated will be from $20kHz$ to $100kHz$ with a maximum input pulse magnitude of $50V_{p-p}$ to the pulse coil. Bias magnetic field will be applied by the use of cylindrical rare earth magnets along the axis of the waveguide. Magnetic biasing will be applied from one direction only, although the magnetism provided will be sufficient to magnetically saturate the waveguide material if necessary.

A ferromagnetic waveguide in excess of five meters in length will be used to construct a test rig to for investigation of signal generation and propagation. This will clearly indicate the amount of attenuation the propagating strain pulse is subject to per unit length of travel.

The performance of the designed acoustic thermometer will be evaluated over the temperature range of 20^oC to 400^oC. This would give a thorough representation of the performance of the instrument because the range exceeds the Curie point for nickel, which is 360^oC. Experiments will be completed in a non-controlled environment and the implementation of automated control circuitry will not be covered.

1.5 Thesis Overview

Chapter 2 focuses on the literature review completed prior to and during the completion of the project. The findings from work completed by others leading to decisions made during the completion of this thesis are given. The chapter also focuses on the theoretical models derived from previous work used to more effectively characterise the system proposed in this thesis.

Chapter 3 gives a detailed description of the test rig used during the investigation of the behavior of acoustic pulses in ferromagnetic waveguides. The electronic circuitry designed for the generation of longitudinal strain pulses in the waveguide and the recovery of the resultant echo signals are described. This chapter discusses the experiments completed to characterise the launch and recovery of longitudinal strain pulses and the propagation of such pulses. The results of the experiments are given and discussed.

Chapter 4 focuses on the implementation of a ferromagnetic waveguide in the design of an acoustic thermometer using the pulse echo technique. Changes made to the hardware to achieve the functionality needed are described and initial results discussed. Optimisation of the acoustic thermometer is discussed and results obtained from temperature measurements given.

In Chapter 5 an error analysis of the results obtained from temperature measurements is shown. The results are compared to expected results from references and the accuracy of the instrument is defined.

Chapter 6 discusses results obtained in Chapter 4 and the analysed results of Chapter 5. The discussion focuses on the research questions and whether all objectives were met. Finally the chapter discusses findings of the research and proposes improvements.

Chapter 2

Literature Review

In this chapter the relevant theory obtained through literature review is summarised.

2.1 Magnetism

A magnetic field is produced whenever an electrical charge is in motion, of which a current carrying conductor is an example. A magnetic field can also be produced by a permanent magnet. In this case there is no motion of electric current involved. A magnetic field is produced by the orbital motions and spins of the electrons, or magnetic moment within the magnet material. Magnetic field strength, H, for a magnetic field generated by a current carrying conductor, has the unit ampere per metre. This emphasises the relationship between magnetic field strength and the generating current [Jiles, 1991].

If a magnetic field is generated in a material, the response of the material to this magnetic field is known as its magnetic induction B, or flux density [Jiles, 1991]. The relationship between the magnetic field and the flux density for a specific material is defined by the permeability μ of the material. The flux density induced in free space, or air, is given as

$$B = \mu_0 H \tag{2.1}$$

where μ_0 is the permeability of free space. For a specific material, its permeability is defined relative to the permeability of free space μ_0 and is known as the relative permeability μ_r. This gives the flux density induced by a magnetic field for a specific material as

$$B = \mu_0 \mu_r H \tag{2.2}$$

The magnetisation of a specific material, M, is defined as the magnetic moment per unit length of the material, and is given by the relation

$$M = \frac{B}{\mu_0} \qquad (2.3)$$

which indicates the magnetism of a specific material can also contribute a flux density without the presence of a magnetic field, as with permanent magnets and magnetised ferromagnetic materials. This gives the total relation for the flux density in a material as

$$B = \mu_0 \mu_r (H + M) \qquad (2.4)$$

If a material is magnetised to a point where all the magnetic moments within the material is aligned parallel to the applied magnetic field, saturation magnetisation M_0 for the material has been reached.

2.2   Magnetostriction

The magnetostrictive effect on a ferromagnetic material with a length far larger than its width is shown in Figure 2.1. The magnetostrictive effect can best be explained if the domain theory is considered [Crawford, 1955].
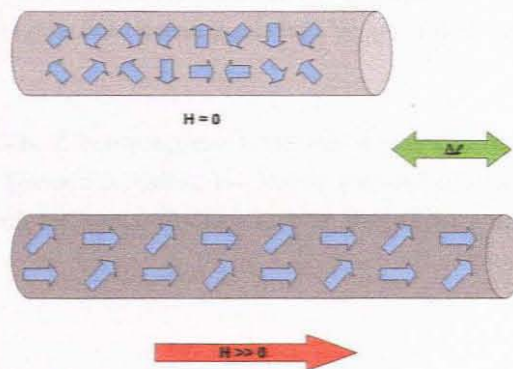
Figure 2.1: The Joule effect on ferromagnetic materials when subjected to a magnetic field

The atoms in every solid media are randomly arranged. Each of these atoms possess a magnetic moment. This is due to their orbital electrons which is its fundamental magnetic

6

particle. The magnetic moment of each atom in the material structure is almost completely canceled by the magnetic moments of adjacent atoms [Crawford, 1955].

Ferromagnetic materials differ from this atomic description of solid materials. The atoms in ferromagnetic materials undergo constant exchanges of force. This results in small atomic domains in the material in which the magnetic fields of the atoms are arranged parallel to one another. These atomic domains are all arranged in different directions within the crystal structure of the material. If an external magnetic field is applied to the material, some of the atomic domains are neutralised, and other grow as the surrounding domains rearrange themselves to align with the applied magnetic field. As the applied magnetic field increases, the crystal structure of the material becomes dominated by one domain of magnetic moment. A further increase in the applied magnetic field sees all the crystal structures within the material, each dominated by a domain of magnetic moment, trying to arrange themselves parallel to the applied magnetic field. As the crystal structures rearranges themselves, the material will undergo a change in physical dimension. The magnitude of this change in physical dimensions is dependent on the type of ferromagnetic material [Crawford, 1955].

If a ferromagnetic material in the form of a thin rod is considered, the change in physical dimension from the magnetostrictive effect will establish itself along the length of the rod. This change in unit length with respect to the length of the material is known as the strain and is given in equation 2.5.

$$\xi = \frac{\Delta l}{l} \tag{2.5}$$

If a large magnetic field is applied to a ferromagnetic material and an increase in magnetic field no longer produces a change in the physical dimensions of the material, saturation magnetostriction has been reached. If an alternating magnetic field is applied to one end of a ferromagnetic rod, a longitudinal strain pulse will be generated that propagates along the axis of the rod.

The magnetostriction of ferromagnetic materials is also affected by elastic stress. This relationship is defined by Young's modulus, Y_0. Young's modulus is by definition the ratio of stress over strain in the region for which Hooke's Law is obeyed for a specific material, and is given by the relation:

$$Y_0 = \frac{\sigma}{\xi} \tag{2.6}$$

where σ is the applied stress and is given as

7

$$\sigma = \frac{F}{A} \tag{2.7}$$

where F is the applied force and A the cross sectional area of the material through which the force is applied. On rearrangement and by substituting for σ and ξ the relation becomes:

$$\frac{F}{A} = -Y_0 \frac{\Delta l}{l} \tag{2.8}$$

Equation 2.8 shows that elastic stress and applied strain are directly dependant on the elastic properties of the material, and that the strain induced by an alternating magnetic field when a longitudinal pulse is launched can be affected by the strain produced by applying tensile stress on the material mechanically.

2.3 Wave Propagation

The propagation of a longitudinal wave in a thin rod can be explained by the one dimensional wave equation for solid materials as derived by Heuter & Bolt [1955], Coulter [1987], Thompson [1978] and Kinsler & Frey [1950].

If one considers a length of solid material, with a width much smaller than that of the wavelength λ of the longitudinal pulse propagating in it, which is stressed uniformly at its ends by the forces F_x and $-F_x$, the longitudinal strain caused by the propagating strain pulse along the x axis of the material is $\frac{d\xi}{dx}$. Equation 2.8 becomes:

$$\frac{F_x}{A} = -Y_0 \frac{d\xi}{dx} \tag{2.9}$$

Rearranging of the equation gives:

$$F_x = -AY_0 \frac{d\xi}{dx} \tag{2.10}$$

If one now considers a small segment of the solid material as illustrated in Figure 2.2, with density ρ and the unstressed length of the section dx. The force at position x is F_x, and the force at $x + dx$ is $F_x + dF_x = F_x + \frac{\partial F_x}{x}dx$. F_x and ξ are both functions of x and time t. Therefore, partial differential coefficients of F_x and ξ can be used. The net tensile force, denoted as $-dF_x$, is given as:
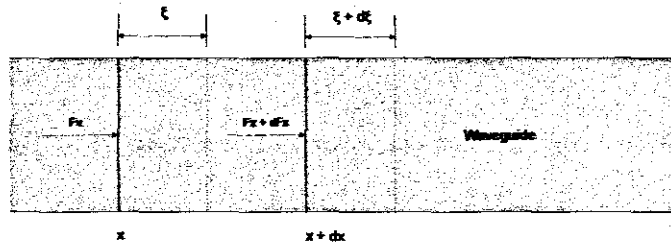
Figure 2.2: The forces and displacements in a thin bar as a result of a propagating longitudinal wave [Coulter, 1987]

$$-dF_x = F_x + \frac{\partial F_x}{\partial x} - F_x dx \tag{2.11}$$

which gives:

$$dF_x = -\frac{\partial F_x}{\partial x} dx \tag{2.12}$$

If F_x on the right hand side is substituted by equation 2.10 one gets:

$$dF_x = AY_0 \frac{\partial^2 \xi}{\partial x^2} dx \tag{2.13}$$

If the mass of the section is $\rho A dx$, then the acceleration $\frac{\partial^2 \xi}{\partial t^2}$ of the segment is given by the equation:

$$\rho A dx \frac{\partial^2 \xi}{\partial t^2} = AY_0 \frac{\partial^2 \xi}{\partial x^2} dx \tag{2.14}$$

Dividing by $A dx$ gives:

$$\rho \frac{\partial^2 \xi}{\partial t^2} = Y_0 \frac{\partial^2 \xi}{\partial x^2} \tag{2.15}$$

which gives:

9

$$\frac{\partial^2 \xi}{\partial t^2} = \frac{Y_0}{\rho} \frac{\partial^2 \xi}{\partial x^2} \tag{2.16}$$

Now if one lets $\frac{Y_0}{\rho} = c^2$, where c is the velocity of sound, the equation becomes:

$$\frac{\partial^2 \xi}{\partial t^2} = c^2 \frac{\partial^2 \xi}{\partial x^2} \tag{2.17}$$

Equation 2.17 is known as the one dimensional wave equation for longitudinal wave propagation in solid media. A complex exponential solution for equation 2.17 in the direction of increasing x is given by Coulter [1987] and Kinsler & Frey [1950]. This solution assumes the vibrations caused by the propagating longitudinal wave has simple harmonic motion, and is given as:

$$\xi = \xi_0 e^{j(\omega t - \frac{\omega x}{c})} \tag{2.18}$$

where ξ_0 is the amplitude of the strain wave and ω is the angular velocity. If $k = \frac{\omega}{c}$, the solution becomes:

$$\xi = \xi_0 e^{j(\omega t - kx)} \tag{2.19}$$

The constant k is also known as the wavelength constant, as $k = \frac{\omega}{c} = \frac{2\pi}{\lambda}$. The particle velocity u, uniform over the cross section of the bar, can be calculated by partially differentiating equation 2.19 with respect to t, which gives:

$$u = \frac{\partial}{\partial t} \xi_0 e^{j(\omega t - kx)}$$

$$= j\omega \xi_0 e^{j(\omega t - kx)}$$

thus

$$u = j\omega \xi \tag{2.20}$$

10

Partially differentiating equation 2.19 with respect to x gives:

$$\frac{\partial \xi}{\partial x} = -jk\xi_0 e^{j(\omega t - kx)}$$

which gives:

$$\frac{\partial \xi}{\partial x} = -jk\xi \qquad (2.21)$$

Now if one look at the force F_x on any cross section of the bar, and consider it in terms of a partial differential coefficient of equation 2.10, F_x becomes:

$$F_x = -Y_0 A \frac{\partial \xi}{\partial x} \qquad (2.22)$$

Substituting from 2.21 gives:

$$F_x = Y_0 A jk\xi \qquad (2.23)$$

The characteristic impedance Z of the bar can now be calculated as:

$$Z = \frac{F_x}{u} \qquad (2.24)$$

Substituting from 2.20 and 2.23 for u and F_x gives:

$$Z = \frac{Y_0 A jk\xi}{j\omega\xi}$$

$$= \frac{Y_0 A jk}{j\omega} \qquad (2.25)$$

for $k = \frac{\omega}{c}$:

11

$$Z = \frac{Y_0 A}{c} \qquad (2.26)$$

and for $c = \sqrt{\frac{Y_0}{\rho}}$:

$$Z = A\sqrt{Y_0 \rho} \qquad (2.27)$$

and for $Y_0 = \rho c^2$:

$$Z = \rho c A \qquad (2.28)$$

2.3.1 Modes of Attenuation

Coulter discusses in great detail the mechanisms of attenuation that the propagating longitudinal wave is subject to Coulter [1987]. He divides the processes of attenuation into two main categories, one in which the energy remains in acoustic form, but suffers a change in direction, mode of propagation or both. The other process of attenuation is internal friction losses, which he specifies as the most significant form of attenuation suffered by a longitudinal wave in a thin bar. The different forms of attenuation as classified by Coulter are shown in Figure 2.3.
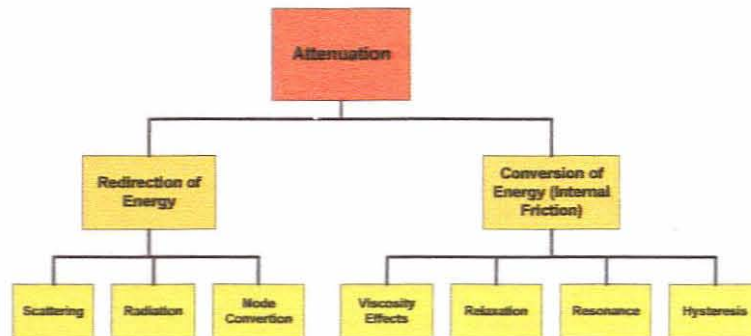
Figure 2.3: The possible processes of attenuation of longitudinal waves in thin ferromagnetic bars [Coulter, 1987]

2.3.2 Magnetostrictive Waveguides

A basic magnetostrictive delay line setup using the pulse echo method is described by Hristoforou [2003] and illustrated in Figure 2.4. The setup consists of a ferromagnetic waveguide, a

12

pulse/excitation coil at the one end and a receive/pick-up coil at the other end. The length of the waveguide is nominally much larger than its width in order to prevent mode conversion of the propagating signal. The ends of the waveguide are terminated in latex adhesive to eliminate acoustic reflections.
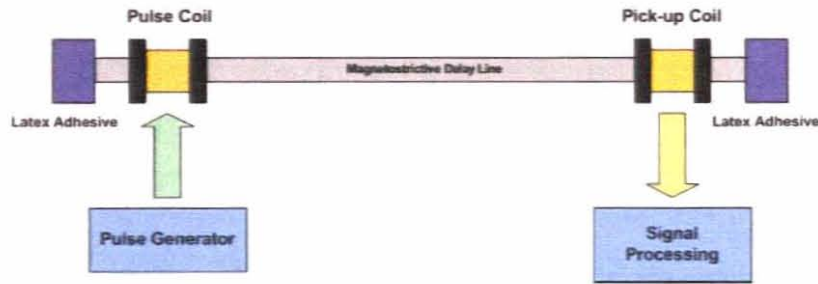
Figure 2.4: The basic magnetostrictive delay line setup [Hristoforou, 2003]

As current is sent through the pulse coil, a magnetic field is induced which in turn produces a flux density within the waveguide material in the region of the pulse coil. A strain is generated in the waveguide because of the Joule effect. If the current supplied to the pulse coil is varied, the induced magnetisation varies, and so too the flux density in the waveguide material and a number of micro strains are generated in the waveguide. These micro strains cause a longitudinal wave to propagate in both directions from the pulse coil along the axis of the waveguide. The longitudinal wave travels through the waveguide at the speed of sound in the relative waveguide material.

The longitudinal pulse propagating along the axis of the waveguide then reaches the pick-up coil. As the section of the waveguide surrounded by the pick-up coil is strained by the propagating longitudinal pulse, it induces a current into the pick-up coil through the Villari effect. This induced current will vary in the same relation as the longitudinal pulse varies, making it possible to retrieve the transmitted longitudinal pulse, although it would have suffered considerable attenuation.

2.3.3   Nickel

Nickel shows relatively high levels of magnetostriction when subjected to a magnetic field, being more than 30 parts per million if the induced strain is considered [Crawford, 1955]. Nickel is relatively cheap, at around 9.50 $US\$kg$, compared to other magnetostrictive materials such as cobalt which costs around 100 $US\$/kg$. Nickel is also readily available for purchase in wire form.

Nickel and its alloys are highly non-corrosive, showing a slow rate of corrosion after prolonged periods of exposure to normal atmospheric elements, losing approximately 8.5% of its total weight due to corrosion over a ten year period in industrial areas where considerable industrial pollution is present [Rosenburg, 1968]. It is for this reason that nickel is extensively used in plating and alloying.
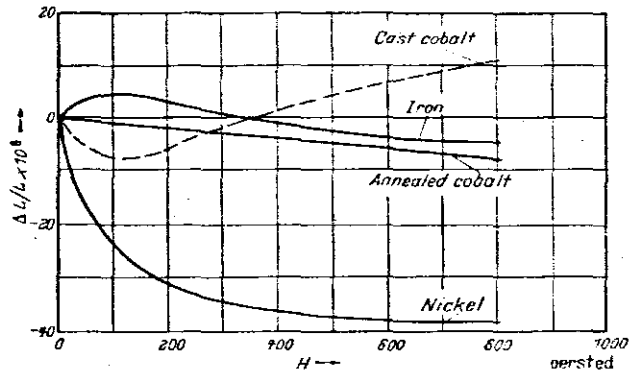
Figure 2.5: Induced strain as a function of magnetic field for nickel and various alloys [Crawford, 1955]
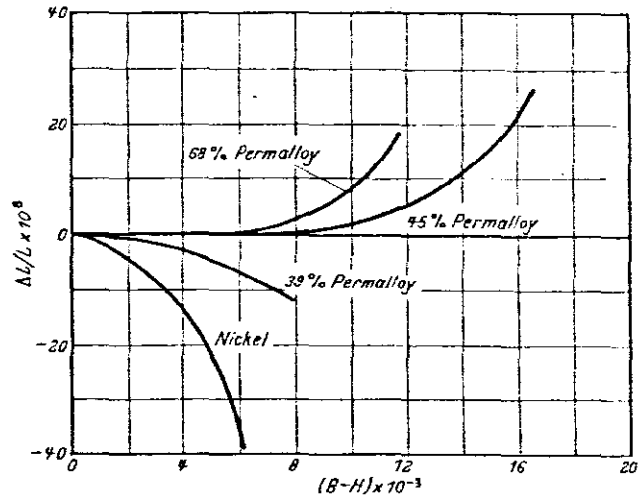
Figure 2.6: Induced strain as a function of magnetization for nickel and various permalloys [Crawford, 1955]

The induced strain for various materials is shown as a function of magnetic field and magnetization in figure 2.5 and 2.6 respectively. The magnetostrictive properties of high purity nickel is shown in figure 2.8. It can be seen from the figures that nickel undergoes negative magnetostriction when placed in a magnetic field. This means that if a thin nickel rod is considered, the rod will decrease in length when placed in a magnetic field. It can also be noted that the magnetostrictive behavior of nickel and its alloys is monotonic. The properties of some relevant materials is listed in Table 2.1.

Nickel has a melting point of $1440^{\circ}C$, and the Curie point for nickel is approximately $360^{\circ}C$. The Curie point is the temperature at which the magnetic properties of the material are no longer present. The elastic properties of nickel as a function of temperature, specifically Young's modulus of elasticity, is shown in figure 2.7 [Rosenburg, 1968]. Young's modulus for pure nickel decreases almost linearly with an increase in temperature.

14
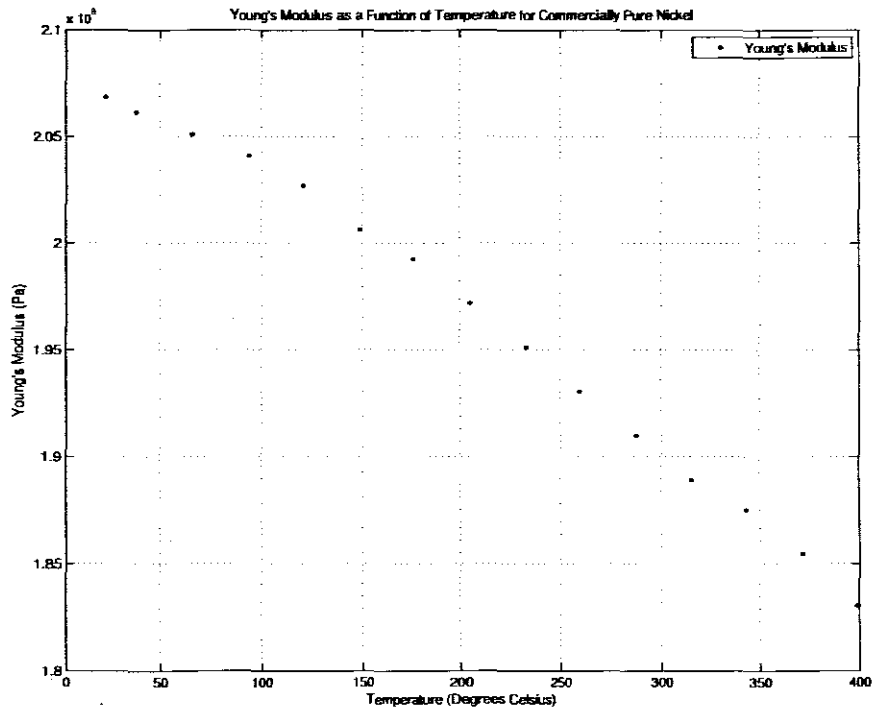
Figure 2.7: Young's modulus as a function of temperature for commercially pure nickel [Rosenburg, 1968]

2.4 Magnetic Biasing

If a ferromagnetic material is placed in a magnetic field, the magnitude of the induced strain differs from one ferromagnetic material to the next. The polarity of the induced strain is not dependent on the polarity of the applied magnetic field, and also differs from one material to the next. The effect an increasing magnetic field has on nickel and permalloy is illustrated Figure 2.8.

If a longitudinal pulse is launched in a pure nickel waveguide by applying an alternating magnetic field using a coil with N number of turns, length of l meters and by supplying the coil with i current, the field strength within the coil would be:

$$H = \frac{iN}{l} \quad Ampere - Turns/m \tag{2.29}$$

This field, which is generated by the current in the coil, will produce a flux density B in the core of the coil, in this case the waveguide. This flux density is given by:

15

Table 2.1: Properties of magnetostrictive materials [Abramov, 1998]

Material	Chemical Composition	Density $(g.cm^{-3})$	Young's Modulus (Y_0) (GPa)	Velocity of Sound $(m.s^{-1})$
Nickel	99% Ni	8.9	206	4800
Permendur	65% Co, 35% Fe	8.2	205	5200
Alfer	12.4% Al, 87.6% Fe	6.7	158	4800
Permalloy	40% Ni, 60% Fe	8.2	130	–
Ferrite	Fe_2O_3	5.3	180	–

Material	Permeability (μ_r)	Magnetostriction Constant $(10^7 N.m^{-1}T)$	Saturation Magnetostriction $(10^{-6})\xi_s$	Curie Temperature (C^o)
Nickel	20 – 50	2.3	−37	360
Permendur	50 – 80	1.5	90	980
Alfer	60 – 100	0.8	40	600
Permalloy	–	0.3	25	–
Ferrite	270	2.3 – 5.5	−9	–

$$B = \mu_r H \quad T \qquad (2.30)$$

where μ_r is the relative permeability of the core material and μ_0 is the permeability of free space.

If the launched longitudinal pulse is recovered by utilising the Villari effect, the frequency of the recovered signal will be double that of the initial launched signal. The reason for this is that for pure nickel a negative strain is induced regardless of the polarity of the applied magnetic field, and nickel contracts for either a positive or negative applied magnetic field.

This contraction occurs for each half cycle of the applied alternating magnetic field, launching a longitudinal strain pulse with a frequency of double that of the alternating magnetic field
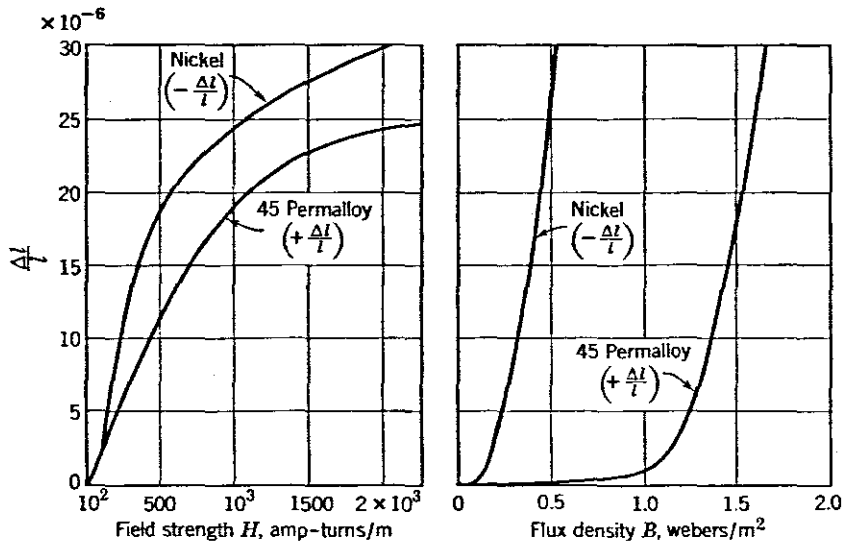
Figure 2.8: The change in length per unit length as a function of field strength for nickel [Heuter & Bolt, 1955]

Coulter [1987]. The frequency doubling effect is illustrated in Figure 2.9 (a).

It can be seen from Figure 2.9 that the applied bias magnetic field has to be larger or equal to that of the applied alternating magnetic field for signal generation. Optimal magnetic bias will be achieved if the gradient for $\frac{d\xi}{dH}$ is high.
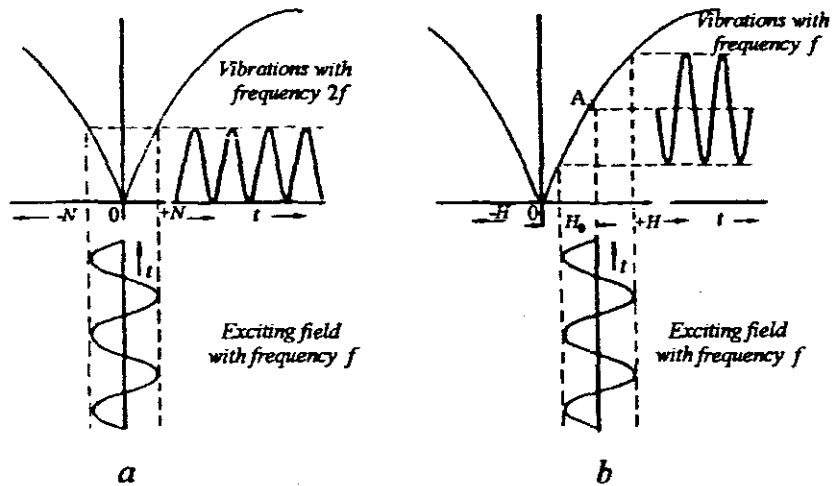
Figure 2.9: Magnetostriction as a result of an alternating magnetic field: (a) no bias magnetic field (b) with bias magnetic field [Abramov, 1998]

The effect of the bias magnetic field is shown mathematically by Coulter [1987], as also shown by Heuter & Bolt [1955] and Gooberman [1969] (p.87). The strain, ξ, induced on the waveguide when subjected to a magnetic field is given as the quadratic equation,

17

$$\xi = \alpha B^2 \tag{2.31}$$

where α is a constant of proportionality and B is the flux density present in the nickel waveguide. As this is a quadratic equation, the strain is independent of the sign of the flux density B. If a bias flux density, B_0, is applied, a static strain, ξ_0, is induced. This gives:

$$\xi_0 = \alpha(B_0)^2 \tag{2.32}$$

If an alternating flux density, B, is superimposed on the bias flux density B_0, a linear effect will be obtained.

Differentiation of equation 2.32 with respect to B_0 gives:

$$\frac{d\xi_0}{dB_0} = 2\alpha B_0 \tag{2.33}$$

Rearranging equation 2.33 gives:

$$d\xi_0 = 2\alpha B_0 dB_0 \tag{2.34}$$

Substituting B for dB_0 and ξ for $d\xi_0$ in 2.34 gives:

$$\xi = 2\alpha B_0 B \tag{2.35}$$

Equation 2.35 is known as the basic magnetostrictive strain equation and $2\alpha B_0$ is known as the magnetostrictive strain constant and has the dimension T^{-1}.

If the waveguide is clamped at both ends while a longitudinal pulse is launched, stress will be developed in the waveguide. The relationship between the incremental stress σ and the incremental flux density B is given as:

$$\sigma = \Lambda B \tag{2.36}$$

18

Λ is the magnetostrictive stress constant with dimension $N.Wb^{-1}$. Applying Hooke's Law to equation 2.36 gives:

$$\sigma = \xi Y_0 \tag{2.37}$$

Now if ξ in equation 2.37 is substituted by ξ as given by equation 2.35 the relationship becomes:

$$\sigma = 2\alpha B_0 B Y_0 \tag{2.38}$$

And substituting in equation 2.38 for σ as given by equation 2.36 gives:

$$\Lambda = 2\alpha B_0 Y_0 \tag{2.39}$$

Equations 2.35, 2.36 and 2.38 are not exact, although the error margin will be small if the bias flux density B_0 is much larger than the superimposed alternating flux density B.

Equations 2.35 and 2.38 show the magnitude of the strain, in the case of a non-clamped waveguide, or the stress, in the case of a clamped waveguide, that is induced in the waveguide is directly proportional to the varying flux density B that is applied to the waveguide. The reason for this being the presence of the bias flux density B_0. In other words, as the applied alternating flux density B swings positive and negative, its effect will be superimposed on the bias flux density B_0. The strain induced in the nickel will also swing positive and negative as the alternating flux density B swings positive and negative as is evident in Figure 2.9.

Therefore, with the presence of a bias flux density B_0 that is much larger than the applied alternating flux density B, the frequency of the longitudinal pulse that is launched into the waveguide will not be double that of the launch pulse.

2.5 Previous Work

The Joule and Wiedemann Effect and the simultanious generation of longitudinal and torsional waves in magnetostrictive materials was studied by Tzannes [1966]. Mathematical modelling of both of the effects was done and he demonstrates the relation between Poisson's Ratio and the stability of the ferromagnetic waveguide with temperature variance. Tzannes conducted his experiments on a ferromagnetic waveguide setup similar to the basic waveguide setup illustrated

19

in Figure 2.4.

The propagation of acoustic waves in a nickel waveguide was studied by Coulter [1987]. Coulter used the pulse echo method to investigate the attenuation acoustic pulses suffer while propagating in a nickel waveguide. He also studied the effects that applying tensile and torsional stress to the waveguide has on the propagating acoustic pulse. Coulter stated the importance of magnetic biasing and discussed the behavior of acoustic pulses when they are reflected at the ends of a waveguide.

Bell completed a study on how the velocity of sound in metals is affected by the temperature of the material using the pulse echo technique [Bell, 1957]. The results Bell obtained during this study for high purity nickel are illustrated in Figure 2.10. It could be seen annealing of the material affected the material's reaction to temperature variance quite considerably. Bell discussed the presence of reverberation noise in the probe section due to multiple reflections of the propagating signal in the waveguide.

TEMPERATURE °C

Velocity temperature curves for high purity nickel.
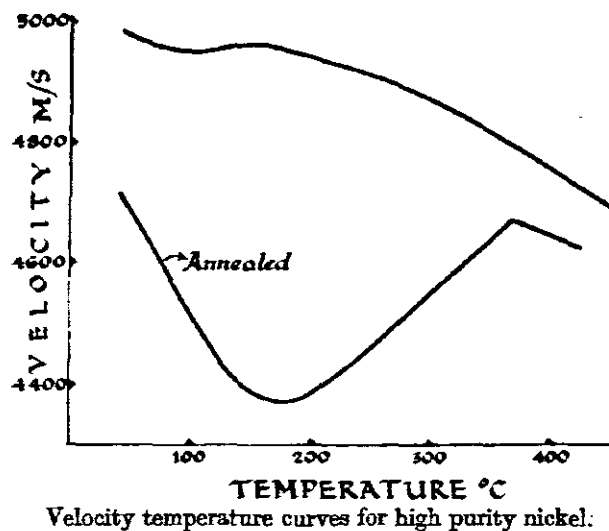
Figure 2.10: The velocity of sound in high purity nickel as a function of temperature [Bell, 1957]

Bell & Mosby [1970] patented an acoustic thermometer based on a ferromagnetic waveguide that utilised the resonance method. The importance of placement of the pulse coil with relation to the transmission end of the waveguide was specified. The non-transmission end of the waveguide was fitted with an acoustic impedance material at a specified distance from the end. This created a discontinuity in the waveguide and isolated the section of the waveguide that functioned as the resonator or specimen. An improved version of this sensor was patented by Bell [1972].

Lynnworth et al. [1965] describes an ultrasonic thermometer based on a ferromagnetic waveguide constructed with nickel wire. The ultrasonic thermometer utilised the pulse echo method and an accuracy of 1% was specified. Lynnworth & Spencer [1970] patented an ultrasonic temperature sensing system that used the pulse echo method. The patent covered multiple arrangements where kinks were made in the waveguide to create a discontinuity that produced

20

partial reflections of the propagating longitudinal waves. This design had the capability of having a number of different sensing sections, giving it ability to give the temperature profile over a larger area as well as measuring dual zones.

Lynnworth [1975] reviewed the industrial applications of ultrasonic sensors. He specified that the temperature dependence of the velocity of sound, c, in materials can be calculated if the density, ρ, and the dependence of Young's modulus, Y_0, on temperature for that specific material were known. This was done with the use of equation 2.40 The review continued to discuss the advances that was made in ultrasonic thermometry and illustrated available solutions.

$$c = \sqrt{\frac{Y_0}{\rho}} \tag{2.40}$$

A computerised system for the characterisation of magnetostrictive materials was presented by Hristoforou et al. [2002]. Hristoforou [2002] developed mathematical models that characterised the generation, propagation and detection of strain pulses in magnetostrictive delay lines.

The literature review completed covered the basic knowledge needed to implement a ferromagnetic waveguide using magnetostriction for signal generation and recovery. The transmission and recovery of longitudinal strain pulses could now be investigated through the construction and investigation of a test rig, which will be examined in the following chapter.

Chapter 3

Optimisation of the Launch and Recovery of Acoustic Pulses in a Nickel Waveguide

This chapter examines the test rig used to investigate and optimise the launch of acoustic pulses in and the recovery of the resultant echo signals from a nickel waveguide. The behavior of the acoustic pulses as they propagate in the waveguide is also studied.

3.1 The Test Rig
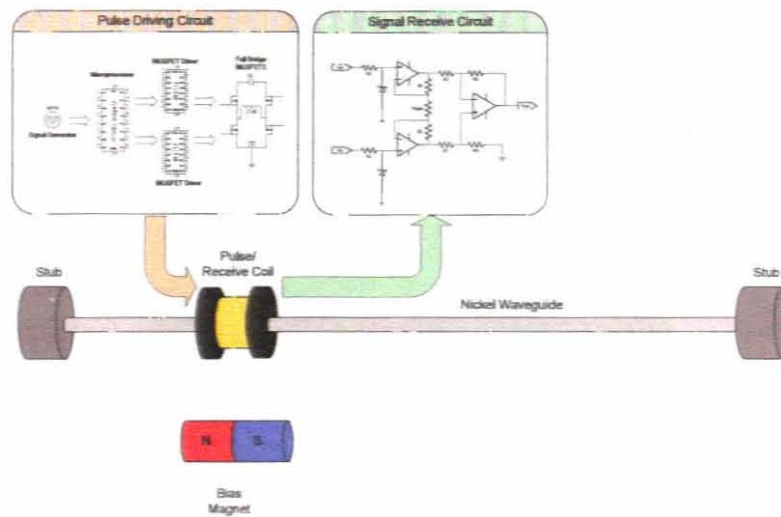
Figure 3.1: A block diagram of the test rig used during the investigation of signal generation and recovery

A block diagram of the test rig used to investigate the launch and recovery of longitudinal strain pulses in nickel is shown in Figure 3.1. The test rig consisted of a length of nickel wire, a transmit/receive or transceiver coil, bias magnets and the necessary electronic circuitry and power supplies.

The nickel wire was supported in an aluminium framework. The framework consisted of a base trunking and five movable elevated clamps, one at each end and three evenly spaced between. The nickel wire was held by the clamps and acoustically insulated with styrofoam pads. A section of the framework is shown in Figure 3.2.
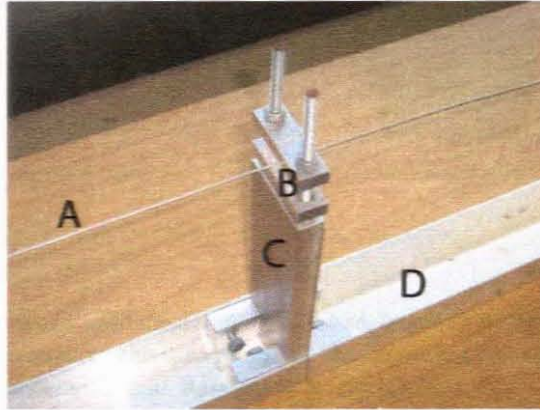
Figure 3.2: A section of the aluminium framework used to support the nickel waveguide. The nickel wire is indicated by (A), (B) indicates the styrofoam pads used for acoustic insulation, an elevated clamp is indicated by (C) and the aluminium trunking is indicated by (D)

The transceiver coil was placed around the nickel wire close to the transmission end. The bias magnets and electronic circuitry was placed on an elevated wooden platform situated underneath the transceiver coil as shown in Figure 3.3.

Figure 3.3: The elevated wooden platform situated underneath the transceiver coil. The power supplies and electronic circuitry is indicated by (A) and (B) respectively. The transceiver coil is indicated by (C). The bias magnets and nickel waveguide is indicated by (D) and (E) respectively

The nickel wire used as acoustic waveguide in the test rig was 99.9% pure unannealed nickel, $2mm$ thick, with a length of $6.52m$. The length of the waveguide was chosen in order to study the behavior of the propagating acoustic pulses. The nickel waveguide was terminated at both

ends with mild steel stubs, which served as high acoustic impedance termination. The acoustic impedance that the termination stub presented to the waveguide, Z_1, the acoustic impedance at the far end of the stub Z_2, the characteristic acoustic impedance of the stub Z_0 and the characteristic acoustic impedance of the waveguide Z_l are indicated in Figure 3.4.
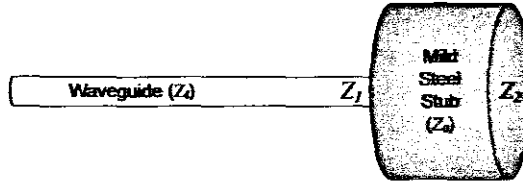
Figure 3.4: An illustration of a mild steel stub used for high acoustic impedance termination. The acoustic impedances presented to the waveguide, at the far end of the stub and the characteristic impedances of the mild steel stub and waveguide is indicated

Coulter [1987] specifies that the length of the stubs be a quarter of a wavelength of the propagating pulse period. When the stub is resonating, it transforms the low impedance Z_2 at its far end into a high impedance Z_1 at the point of termination. This relationship is given as:

$$Z_1 = \frac{Z_0^2}{Z_2} \qquad (3.1)$$

In order to present a large acoustic impedance to the nickel wire, the impedance at the terminating end of the stub Z_1 must be much larger than the characteristic impedance of the waveguide Z_l.

$$Z_1 >> Z_l \qquad (3.2)$$

Substitution gives:

$$\frac{Z_0^2}{Z_2} >> Z_l \qquad (3.3)$$

The inequality in 3.3 can easily be satisfied, as the far end of the stub is coupled to air, Z_2

will be so small it can be neglected, and the characteristic acoustic impedance of the stub can be made much larger than that of the nickel wire.

If $Z_2 = 0$, and for a varying signal wavelength, Z_1 can be given as:

$$Z_1 = jZ_0 \tan 2\pi \frac{\ell}{\lambda} \tag{3.4}$$

Where ℓ is the length of the stub. It can be seen from equation 3.4 that, if the wavelength, λ, varies from the wavelength required for the stub to be at resonance, the values of Z_1 and Z_0 also varies directly proportional to each other. Z_0 must, therefore, be large. The reason for this being to ensure a large enough deviation in wavelength is possible, without risking that Z_1 decreases to the point where it no longer satisfies the relation $Z_1 >> Z_l$.

If one considers equation 2.28, a high value for Z_0 can be ensured if the cross sectional area A of the stub is made large, and a material with a high value of ρc, like steel or tungsten is used. To calculate the length of the stub for a given frequency range, equation 3.4 needs to be re-written.

$$Z_1 = jZ_0 \tan \frac{\pi}{2} \frac{4\ell}{\lambda_{(min)}} \tag{3.5}$$

λ_{max} and λ_{min} are the maximum and minimum wavelengths of the covered frequency band, and Z_1 will have equal values at both these extremes, although one would be opposite in sign, because Z_1 is complex. From this is found:

$$jZ_0 \tan \frac{\pi}{2} \frac{4\ell}{\lambda_{max}} = -jZ_0 \tan \frac{\pi}{2} \frac{4\ell}{\lambda_{min}} \tag{3.6}$$

Dividing by jZ_0 gives:

$$\tan \frac{\pi}{2} \frac{4\ell}{\lambda_{max}} = -\tan \frac{\pi}{2} \frac{4\ell}{\lambda_{min}} \tag{3.7}$$

and for any angle θ:

$$\tan(\frac{\pi}{2} - \theta) = -\tan(\frac{\pi}{2} + \theta) \tag{3.8}$$

25

or:

$$\tan \frac{\pi}{2}(1 - \Delta) = -\tan \frac{\pi}{2}(1 + \Delta) \tag{3.9}$$

where $\Delta = \frac{2\theta}{\pi}$

From 3.9:

$$1 - \Delta = \frac{4\ell}{\lambda_{max}} \tag{3.10}$$

$$1 + \Delta = \frac{4\ell}{\lambda_{min}} \tag{3.11}$$

Adding these equations gives:

$$2 = 4\ell(\frac{1}{\lambda_{max}} + \frac{1}{\lambda_{min}}) \tag{3.12}$$

so that in terms of ℓ:

$$\ell = \frac{1}{2}\frac{\lambda_{max}\lambda_{min}}{\lambda_{man} + \lambda_{min}} \tag{3.13}$$

The frequency range the stub was designed for was 20kHz to 100kHz. The bulk velocity of mild steel is given as $c_b = 5850ms^{-1}$. Therefore, the maximum and minimum wavelengths were:

$$\lambda_{max} = 292.5 \times 10^{-3}m$$
$$\lambda_{min} = 58.5 \times 10^{-3}m$$

giving a calculated stub length ℓ of:

$$\ell = 24.375 \times 10^{-3} m$$

The high impedance termination stubs also served a mechanical purpose. Some experiments required the entire waveguide be put under tensile stress. Custom brackets were constructed that fitted behind the mild steel stub on the one end of the waveguide, linking it with a scale that was connected to a rod and nut. On the other end the stub was clamped into the structure holding the waveguide. This made it possible to precisely adjust the tensile stress over the waveguide by adjusting the nut on the rod. The brackets used to hold the waveguide and to apply tension to the waveguide is illustrated in Figure 3.5.
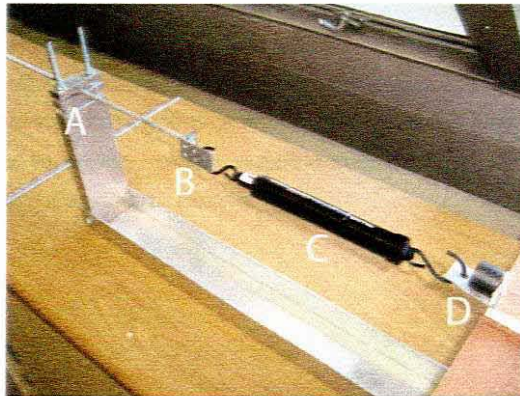
Figure 3.5: The custom brackets used to apply tensile stress to the nickel wire and the scale used to measure the applied tensile stress. The elevated clamp holding the rod and adjusting nut is indicated by (A). The bracket connecting the scale to the adjusting rod is indicated by (B). (C) indicates the in line scale and the bracket connecting the scale to the nickel waveguide is indicated by (D), acoustically insulated with styrofoam

3.1.1 The Pulse Driving Circuit

To fully investigate the behavior of acoustic pulses in a nickel waveguide, a pulse driving circuit was designed with the ability to generate a burst pulse variable in frequency, pulse repetition frequency and amplitude. The number of pulses per pulse burst was also variable. The driving circuit had the ability to supply sufficient current to excite the transceiver coil.

Coulter [1987] and Glover *et al.* [1968] showed an optimum frequency band between $20kHz$ and $100kHz$. Using their work as a guide, this bandwidth was selected to investigate. The pulse repetition frequency range had to be variable between $10Hz$ and $300Hz$ in order to allow for propagating signals to completely attenuate before the next series of strain pulses is launched in the nickel wire, thereby eliminating standing waves.

The magnitude of the pulse generated by the driving circuit was made variable in order to investigate the efficiency of the transmit coil, the effects of magnetic biasing and to characterise

the magnetostrictive effect for the nickel wire. The power supply used by the pulse driving circuit supplied a maximum voltage of $25V_{DC}$ and maximum continuous current of 5A. The voltage supplied by the power supply was switched in polarity over the transmit coil with the use of four N-channel Mosfets in a full bridge configuration, giving the pulse driving circuit the ability to drive the transceiver coil with a constant voltage of up to $50V_{p-p}$.

The number of pulses per pulse burst was made variable to investigate whether more pulses per pulse burst had an effect on the magnitude of the launched acoustic pulse and to establish the optimal number of pulses per pulse burst for signal generation. The driving circuit was capable of generating up to 50 pulses per pulse burst, which was deemed sufficient for experimental purposes.

At first, a circuit was designed that utilised a voltage controlled oscillator and logic circuits to generate the pulse burst. The pulse burst would then be used to drive the full bridge mosfet configuration. This circuit was unable to generate exact signal frequencies, because the signal generated by the voltage controlled oscillator was scaled down with an 8-bit counter. The circuit was also time consuming to adjust, as the variable voltage supplied to the voltage controlled oscillator was adjusted by two potentiometers.
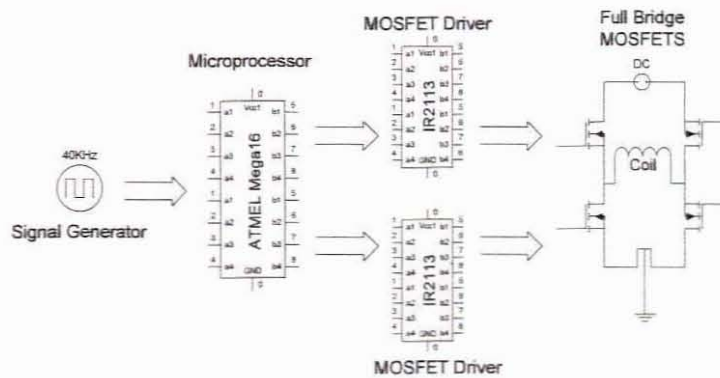
Figure 3.6: Functional block diagram of the pulse driving circuit.

The above mentioned circuit was replaced with a micro-controller that reacted to a digital input signal; in this case a signal generator was used. The micro-controller was programmed to generate an interrupt on each positive change of the input voltage from the signal generator. The interrupt routine would then determine the status of the output port of the micro-controller used to drive the full bridge mosfet configuration. This was achieved by implementing a count variable which was decreased by one with every instance of the interrupt routine. This meant that the pulse burst used to drive the full bridge mosfet configuration could be controlled to

28

a single pulse, and adjustments to frequency and pulse repetition frequency could be made by simply changing the output frequency of the signal generator, or editing a variable in the microcontroller software. A block diagram of the driving circuit that was used is illustrated in Figure 3.6.

This circuit could easily have been replaced with a signal generator and some logic circuits, but the fact that a single coil was utilised to pulse and receive the acoustic pulses and their echoes, meant that all the gates of the Mosfets in the full bridge configuration over the coil had to be opened. The reason for this was to ensure the coil was floating. The circuit was capable of driving each gate of the Mosfets separately.

Four outputs from the micro-controller was used to trigger two IR2113 Mosfet driver integrated circuits. The IR2113 Mosfet driver integrated circuits in turn provided the necessary gate current to drive the Mosfets. After the coil was driven by the Mosfet bridge, none of the Mosfets was activated, ensuring that the coil was floating to not interfere with the pick up of echo signals.

3.1.2 The Transceiver Coil

In order to generate the maximum amount of strain in the nickel wire during the launch of acoustic pulses, the transceiver coil had the ability to induce a large enough magnetic field into the nickel wire. The dimensions of the coil as wound on a machined nylon former is illustrated in Figure 3.7.

The length, ℓ, of the coil had to be equal to or shorter than $\frac{1}{4}\lambda$ of an acoustic pulse in nickel to ensure that the acoustic pulse was launched without self-interference from the transmit coil [Coulter, 1987]. The pulse wavelength was at its shortest when pulse frequency was at its highest, therefore ℓ was calculated for a pulse frequency of $100kHz$.

$$4\ell = \frac{1}{100000} \times 4900$$
$$= 0.049$$
$$\ell = 0.01225 \ m$$

The inside radius of the coil former, b, was also fixed at $4mm$, as it was impossible to machine the former any further without compromising its structural integrity.

Saturation induction, B_s, for commercially pure nickel was given as $6.17 \times 10^{-1}T$ [Rosenburg, 1968]. Induction, or flux density, could also be expressed by the following formula [Jiles, 1991].
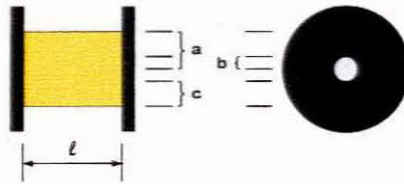
Figure 3.7: An illustration of the dimensions used during the design of the transceiver coil

$$B = \frac{\Phi}{A} \tag{3.14}$$

Where A is the cross sectional area of the material and Φ is the magnetic flux passing through the material. The cross sectional area of the nickel wire was calculated as 9.86×10^{-6}. The magnetic flux at saturation induction was calculated using equation 3.14.

$$B_s = \frac{\Phi_s}{A}$$
$$\Phi_s = B_s \times A$$
$$= 6.015 \times 10^{-6} \ Wb$$

An equation for the flux density in a solenoid was reduced by Kraus & Carver [1973] and given as:

$$B = \frac{\mu N I}{\ell} \tag{3.15}$$

where N is the number of turns in the coil windings and I is the current passing through the coil. The specifications of the pulse driving circuit stated that a maximum current of $5A$ could be drawn from the power supply. If equation 3.15 is manipulated and the known values of B, I, ℓ and μ are used, the number of turns required for the coil can be calculated.

$$N = \frac{\ell B_s}{\mu \mu_r I}$$
$$= \frac{0.01225 \times 0.61}{600 \times 4\pi \times 10^{-7} \times 5}$$
$$\approx 25 \ Turns$$

A general equation for the inductance of a coil in terms of N, Φ and I was given by Bird [2003]:

$$L = \frac{N\Phi}{I} \qquad (3.16)$$

which gives the calculated inductance needed for the coil as:

$$L = \frac{25 \times 6.015 \times 10^{-6}}{5}$$
$$= 30.075 \times 10^{-6} \ H$$

The transceiver coil was then wound using $2.5mm$ thick coated copper wire for the windings. After the coils was wound, their dimensions and properties were measured. The dimensions of the transceiver coil was:

$$\ell = 12.25mm$$
$$a = 16mm$$
$$b = 4mm$$
$$c = 12mm$$
$$N = 25$$

The inductance of the coil was measured using a HP 4129A LF impedance analyser and the measured inductance at $30kHz$ was $33.52\mu H$, which was close to the calculated value and sufficient for the purpose of the coil.

The position of the coil with respect to the transmission end affects both the launch and recovery of acoustic pulses in the waveguide, because of interference from echo signals reflected from the transmission end. For this reason a single coil was used to launch and recover acoustic pulses in the nickel wire. This also ensured the impedance of the coil was the same for signal transmission and recovery. A picture of the coil and former used is shown in Figure 3.8.

The coil was supplied with a burst of alternating current from the pulse driving circuit. As

31
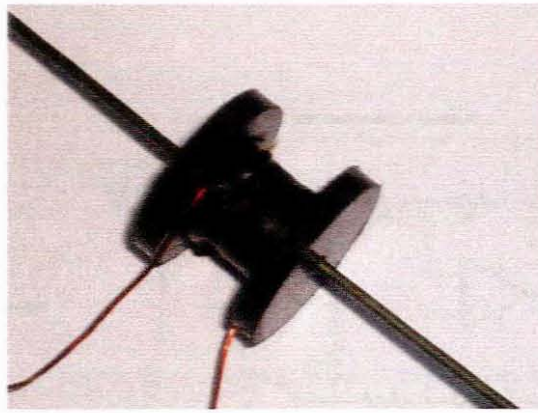
Figure 3.8: The transceiver coil and former used for acoustic pulse generation and recovery.

the current flowed through the coil, a magnetic field was induced that alternated in magnitude and polarity as the supplied current alternated. The alternating magnetic field produced a strain in the nickel wire which also alternated at the same frequency as that of the supplied current, causing a longitudinal strain pulse to propagate along the axis of the waveguide in both directions from the coil, as defined in Section 2.3.

3.1.3 The Receive Circuit

The receive circuit was also connected over the transceiver coil and consisted of a clipping circuit and an instrumentation amplifier. The clipping circuit was implemented as a safeguard to the inputs of the instrumentation amplifier, as its inputs could only handle a maximum input voltage of $15V$ and the magnitude of the driving pulse burst could be up to $25V$. A circuit diagram of the receive circuit is shown in Figure 3.9.

After the coil was driven by the pulse driving circuit, the coil's terminals were floating. This made it especially difficult to design and construct a clipping circuit that worked well without attributing noise to the input stage of the instrumentation amplifier. The reason for this being that the inputs to the instrumentation amplifier was differential and the clipping circuit was referenced to ground.

The instrumentation amplifier used was an integrated circuit from Analog Devices, the AD624. This instrumentation amplifier IC was easy to configure and offered a gain of up to 1000. It had a minimum common mode rejection ratio of 130dB at a gain of 500 to 1000 and a gain bandwidth product of $25MHz$. The outputs of the instrumentation amplifier was fed to an Agilent digital oscilloscope, which had the ability to sample data and store it onto an USB flash drive, or to a personal computer via the USB interface.
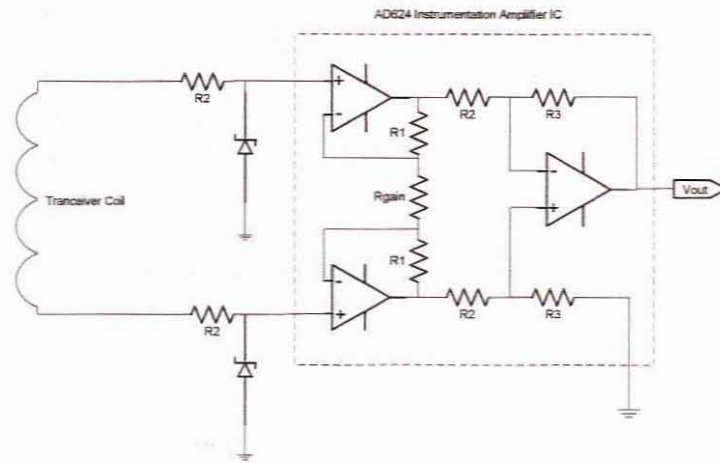
Figure 3.9: Functional block diagram of receive circuit

3.2 Test Rig Investigation

This section looks at the experiments completed on the test rig to optimise the launch and recovery of acoustic pulses in the nickel waveguide.

3.2.1 Initial Findings

One of the initial recovered echo signals is shown in Figure 3.10. It was observed that only a single echo pulse was present and the magnitude of this pulse was small. This indicated that the ultrasonic pulse launched did not produce sufficient strain, or was subject to interference. The transceiver coil was positioned at $\frac{1}{4}\lambda$, and the driving pulse magnitude was $30V_{p-p}$. This meant sufficient power was supplied to the transceiver coil. It was speculated interference was the reason for the poor echo pulse magnitude and it was decided to first investigate the correct coil position.

3.2.2 Determining the Correct Coil Position

The correct placement of the transceiver coil with respect to the transmission end of the waveguide was important as the reflection of the launched pulse from the transmission end of the waveguide could interfere with the launched pulse if they were out of phase. Coulter [1987] specified that the termination of the transmission end of the waveguide, whether the transmission end was held or not, determined the correct position for the transceiver coil. He specified
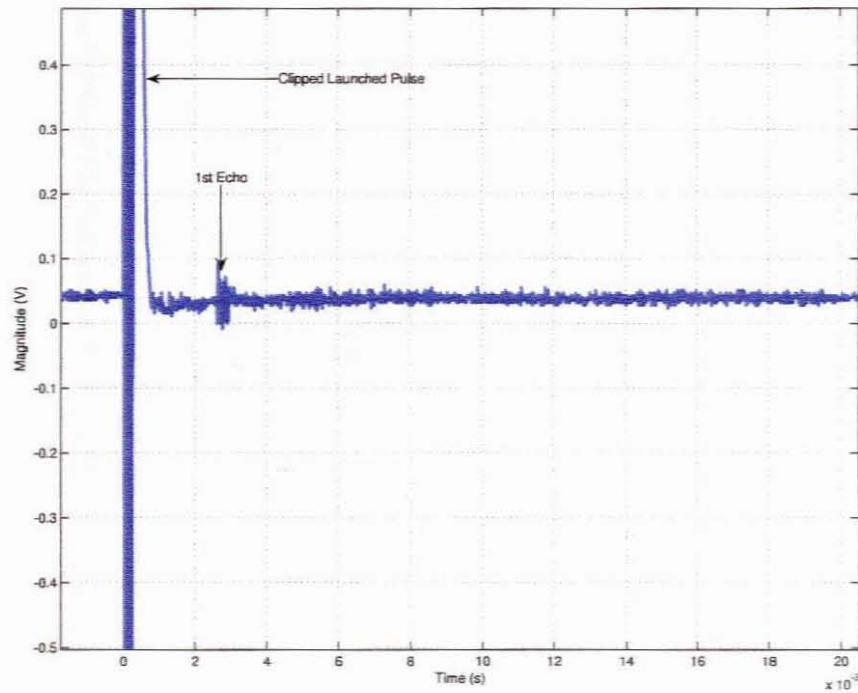
Figure 3.10: An initial recovered echo signal, showing only one small echo pulse (40kHz Input Pulse Frequency)

if the end of the waveguide where reflection took place was not fixed, in other words not terminated at the end and a displacement of the waveguide was possible, the propagating pulse would undergo a 180° phase shift. Therefore, the centre of the transceiver coil should be situated $\frac{1}{4}\lambda$ of the launched pulse in nickel from the end of the waveguide. This would ensure the reflected pulse was in phase with the launched pulse and add to its magnitude. If the end of the waveguide was not fixed and no displacement could take place, the reflected pulse would not undergo any phase shift. In this case the centre of the transceiver coil sould be situated $\frac{1}{2}\lambda$ from the end of the waveguide for the reflected pulse to be in phase with the launched pulse.

The transceiver coil was placed at $\frac{1}{4}$, $\frac{1}{2}$, $\frac{3}{4}$ and full wavelength from the transmission end of the waveguide and the recovered echo signals for the frequencies 20KHz, 30KHz and 40KHz was investigated. It was found that, with the centre of the transceiver coil at $\frac{1}{2}\lambda$ from the transmission end of the waveguide, and for all pulse frequencies investigated, that the amplitude of the recovered signal echo was highest. The magnitudes of the second, third and fourth echoes increased, indicating there was an increase in the magnitude of the acoustic pulse that was launched. This also indicated the nickel wire used in the test rig did in fact behave as a fixed waveguide, because it was terminated in high acoustic impedance mild steel stubs. A recovered echo signal where the transceiver coil was in the $\frac{1}{2}\lambda$ position is shown in Figure 3.11.

34
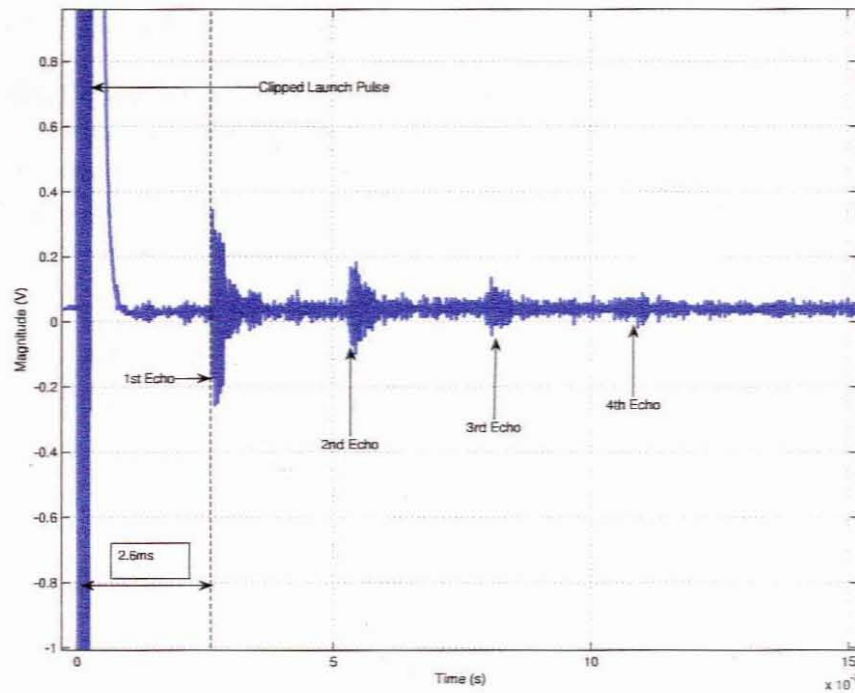
Figure 3.11: A recovered echo signal where the transceiver coil was moved to half of a wavelength of the launched pulse in nickel. The time delay between the launch pulse and the first echo pulse is indicated (40kHz Input Pulse Frequency)

3.2.3 Signal Verification

Signal verification was done to confirm the recovered echo signals were a result of the launched acoustic pulse. This was verified in two ways, the first being to calculate the time of flight of the propagating pulse and comparing it with the time delay between the driving pulse and the first recovered echo pulse. This was effected using the equation 3.17.

$$t_{of} = \frac{D}{\nu} \tag{3.17}$$

where D is the distance traveled by the signal and ν is the velocity at which the signal travels. The distance the signal traveled would be equal to twice the distance from the centre of the transceiver coil to the non-transmission end of the waveguide, because the first signal echo expected was the reflection of the acoustic pulse from the non-transmission end of the waveguide. The centre of the transceiver coil was situated $80mm$ from the termination stub at the transmission end of the waveguide. This distance was equal to $\frac{1}{2}\lambda$ of an acoustic pulse in nickel with a pulse frequency of $30kHz$. The distance traveled by the signal was calculated

35

as 12.88m. This gave a calculated time of flight of 2.63ms. This result can be compared with Figure 3.11 where the time delay between the launched pulse and the first echo is indicated. It could also be seen signal echoes occurred at time intervals of slightly more than 2.5ms.

Secondly, the frequency of the return signal could be investigated. If no bias magnetic field was present at the transceiver coil, the frequency of the return pulse would be double that of the input pulse burst frequency and if a significant bias magnetic field was applied, the frequency of the return pulse would be equal to that of the input pulse burst frequency. This occurrence is illustrated in Figure 3.20.

3.2.4   Bias Magnet Strength Measurements
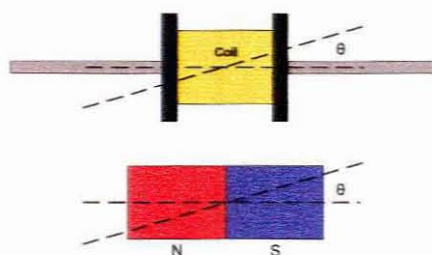
Figure 3.12: Illustration of the correct angle to apply bias magnetic field
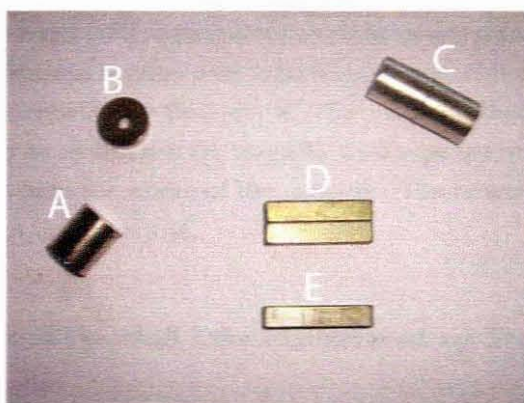
Figure 3.13: The rare earth magnets investigated to be used as bias magnets. A single cylindrical magnet is illustrated by (A), (B) shows a flat cylindrical magnet with a hole. Two joined cylindrical magnets is shown by (C). Two joined rectangular magnets are shown by (D) and (E) illustrates a single rectangular magnet.

The magnetic field strength provided by the bias magnets had to be quantified prior to the investigation of the effect that magnetic biasing would have on the launch and recovery of the acoustic waves. To achieve optimal biasing of the waveguide area covered by the transceiver coil, the magnetic field had to be uniform and parallel to the axis of the waveguide. The correct angle for applying a bias magnetic field is illustrated in Figure 3.12.

Rare earth magnets of various shapes and sizes was acquired for the purpose of magnetic biasing. The uniformity of the magnetic field that the magnets supplied was investigated. This was achieved by measuring the magnetic field strength at the centre and along the axis of the magnets to establish which shape magnet had the greatest region of uniform magnetic field. Magnetic field strength was measured using a model 5080 Gauss Meter by FW Bell. Measurements were verified with a Hall Effect sensor. The Hall Effect sensor used was an A1302 ratiometric linear Hall Effect sensor from Allegro Micro Systems. The different magnets investigated are shown in Figure 3.13. It was found that the cylindrical magnets contributed the highest amount of uniform flux density.
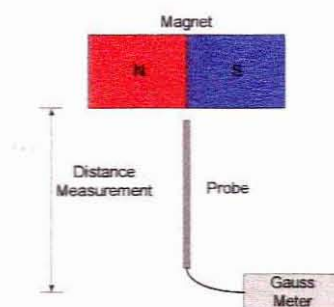
Figure 3.14: The method used to measure the magnetic field strength of the rare earth magnets used for magnetic biasing

The method used to measure the magnetic field strength of the rare earth magnets used for magnetic biasing is illustrated in Figure 3.14. A single cylindrical magnet supplied the highest level of flux density at its center, although it dropped of sharply towards the edges of the magnet. This showed a single cylindrical magnet contributed high levels of flux density to a small area. Two of these cylindrical magnets were then joined. The two cylindrical magnets contributed less maximum flux density at its centre, but the magnetic field supplied was more uniformly spread, and higher at a distance from the centre of the magnets. The measured results obtained with the Gauss Meter is shown in Figure 3.15.

3.2.5 Measurement of the Hall Effect Generated by Transceiver Coil

The magnetic field that the transceiver coil induced whilst being driven had to be quantified prior to the investigation of the effects of magnetic biasing. Two measurements were completed. Firstly the driving voltage to the transceiver coil was kept constant and the frequency of the pulse burst was changed. This was done to characterise the performance of the transceiver coil over frequency. A screenshot of the oscilloscope showing the Hall Effect sensor measurement taken from the side of the coil is shown in Figure 3.16. On inspection of Figure 3.16 the results indicated an integral response to the driving square wave. The reason for this was that a magnetic field was only induced while there was a change in current flowing through the transmit coil. It was found that as the frequency increased the total amount of alternating flux density generated by the transceiver coil decreased. The results obtained from this experiment
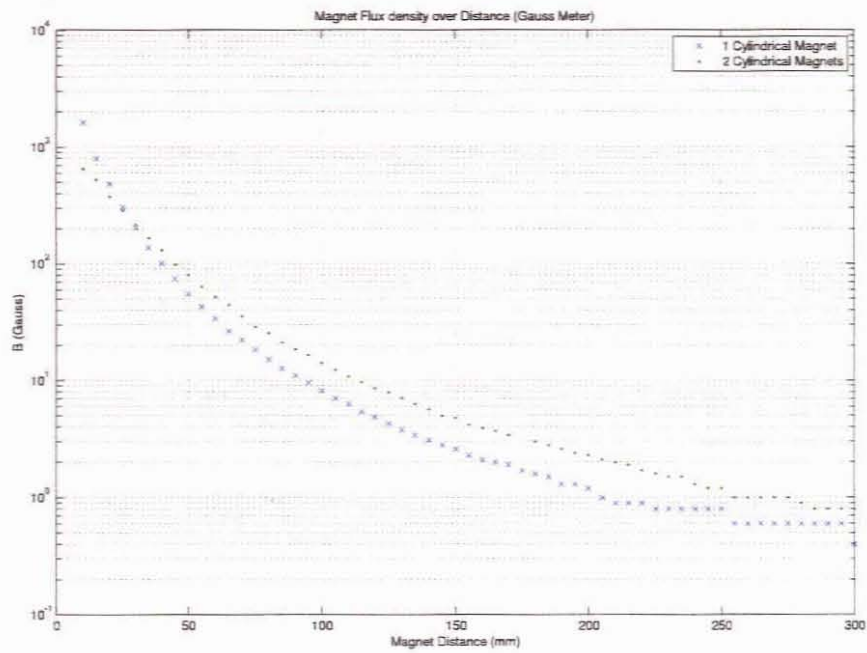
Figure 3.15: Magnetic field strength of the rare earth magnets as measured by the method illustrated in Figure 3.14

Figure 3.16: An oscilloscope screenshot of the output of the Hall Effect sensor placed at the side of the transceiver coil. The driving pulse frequency and magnitude was 20kHz and 20Vp-p respectively

are shown in Figure 3.17.

The reason for the decrease in generated flux density as the frequency of the pulse burst driving the coil increased was because the impedance of the coil increased. This was because the inductance of the coil remained constant and the power source supplied a constant voltage to the transceiver coil. As the impedance of the transceiver coil increased, less current was drawn and a smaller magnetic field was induced. The impedance of the transceiver coil was measured
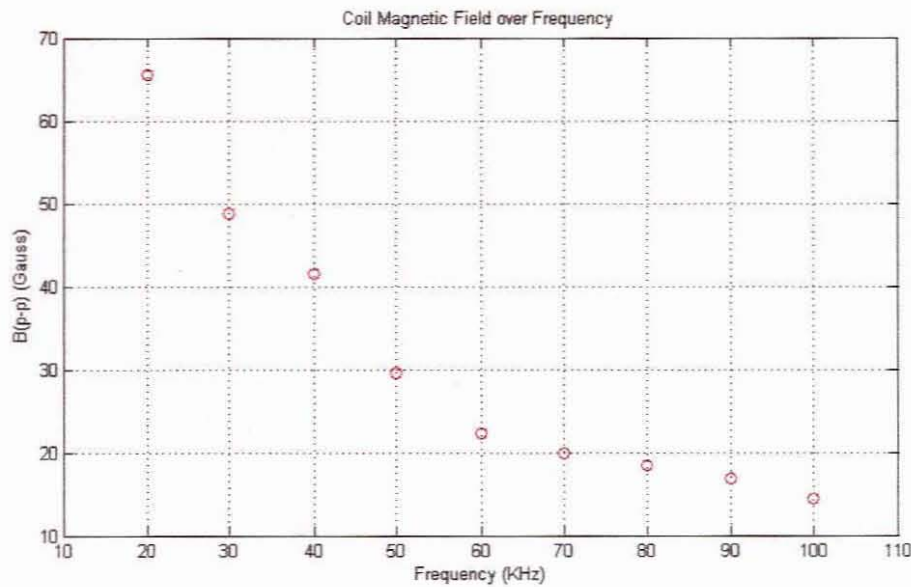
Figure 3.17: The flux density generated by the transceiver coil as a function of frequency

using a Hewlett Packard 4129A LF impedance analyser, over the frequency range of $20kHz$ to $100kHz$. The result of this measurement is shown in Figure 3.18

Secondly the frequency of the input pulse burst was kept constant and the magnitude of the driving pulse was varied. It was found that within the range of the pulse driving circuit, being 5Vp-p to 50Vp-p, the total alternating flux density generated increased linearly as the driving pulse magnitude increased. The reason for this being that the impedance of the coil remained constant while the power driving the transceiver coil increased. The result of this experiment is shown in Figure 3.19.

3.2.6 The Effect of Magnetic Biasing

The magnetic fields contributed by the bias magnets and the transceiver coil was quantified and the effect of magnetic biasing on the launch and recovery of acoustic pulses in the nickel waveguide could be investigated. The magnetic field required for optimal magnetic biasing of the nickel waveguide used in the test rig was established. This was achieved by keeping the magnitude and frequency of the pulse burst supplied to the transceiver coil constant and observing the recovered echo signals while applying a bias magnetic field to the region of the waveguide where the transceiver coil was situated. The bias magnetic field was applied as described in Section 3.2.4 and illustrated in Figure 3.12. The magnitude of the driving pulse burst was kept constant at $30Vp-p$ during this investigation. The magnitude and frequency of the recovered echo signals were investigated and sampled.

Three instances of the first echo pulse are shown in Figure 3.20. A bias magnetic field was applied systematically. The frequency of the input pulse burst was $30kHz$. On investigation of

39
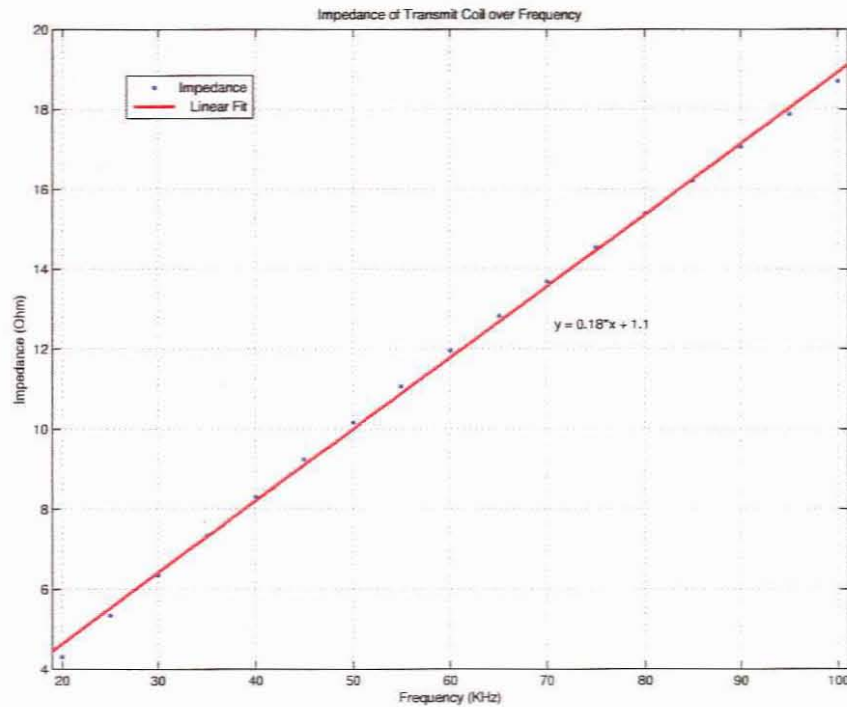
Figure 3.18: The impedance of the transceiver coil for the range of frequencies between 20kHz and 100kHz

Figure 3.20 it was found that for the echo signal where no magnetic biasing was applied, the frequency of the echo signal was equal to $60kHz$. It is shown where an optimal bias magnetic field is applied, the frequency of the echo pulse is equal to $30kHz$ and the magnitude of the echo pulse increased dramatically. The effect that excessive magnetic biasing has on the echo pulse is also shown in Figure 3.20. The magnitude of the echo pulse decreased, indicating that less strain was induced in the nickel wire during the launch of the acoustic pulse, although doubling of the signal frequency have been successfully eliminated.

The magnitude of the first recovered echo pulse was recorded with varied levels of magnetic biasing. The result is shown in Figure 3.21, fitted with a double exponential equation to quantify the effects of magnetic biasing for a $30kHz$ driving pulse. It is shown there was a sharp increase in the magnitude of the first recovered echo pulse as an initial bias magnetic field was applied. This trend continued exponentially to the point where a bias flux density of $0.34T$ was applied. The gradient of the increase in echo pulse magnitude with relation to the applied bias field decreased from this point until it became zero at a bias flux density of $0.63T$. This indicated saturation had occurred and optimal magnetic bias established. The applied bias flux density at which saturation occurred was similar to the value of saturation flux density given by Rosenburg [1968] of $0.614T$. It is shown that further increase in bias magnetic field decreases the echo pulse magnitude, indicating that less strain was induced during the launch of acoustic pulses. The reason for this being the initial strain induced by the bias magnetic field is almost equal to the

40
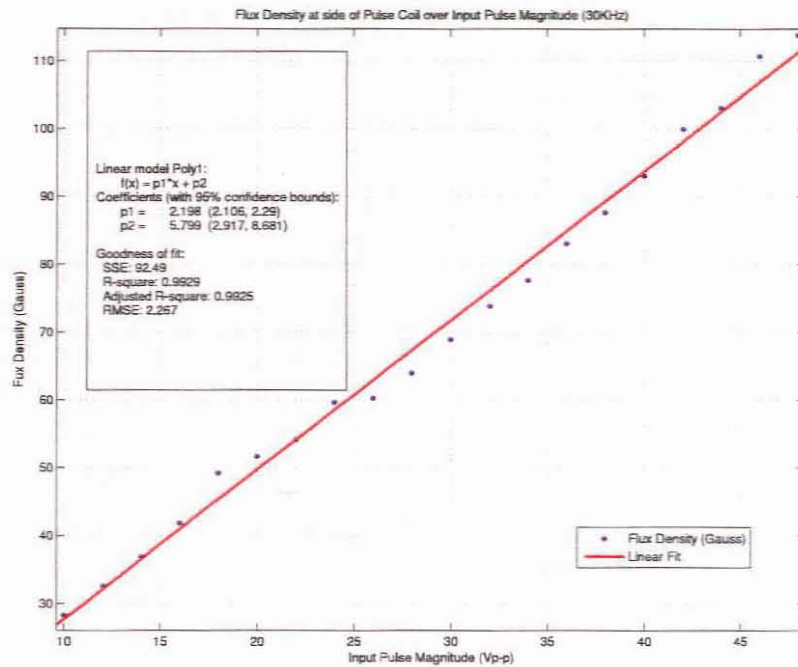
Figure 3.19: The flux density generated by the transceiver coil as a function of the driving pulse magnitude

maximum inducible strain for nickel, limiting the strain induced by the alternating magnetic field added to the bias magnetic field by the transducer coil.

An interesting observation of the effects of magnetic biasing was the phase of the transmitted pulse could be reversed by changing the orientation of the bias magnetic field. It was also found that a section of the waveguide could be permanently magnetised by bringing the bias magnet in contact with that section, or after prolonged exposure. This magnetisation was not permanent, and to ensure the bias magnetic field remained constant, bias magnets were used during all further experimental work.

3.2.7 The Magnitude of the Driving Pulse

The effect of magnetic biasing on the launched acoustic pulse was investigated and quantified. The effect that increased power to the transceiver coil during the launch of acoustic pulses had on the recovered echo signals was investigated. This investigation was done to quantify the magnetostriction induced by the transceiver coil and to find an optimal driving pulse magnitude. The magnitudes of all recovered echo pulses were logged for each incremental increase in power to the transceiver coil, while all other input parameters remained constant. The driving pulse burst frequency was $30kHz$. The applied bias flux density was half of the established optimal level, to ensure saturation would not occur during the investigation.

41
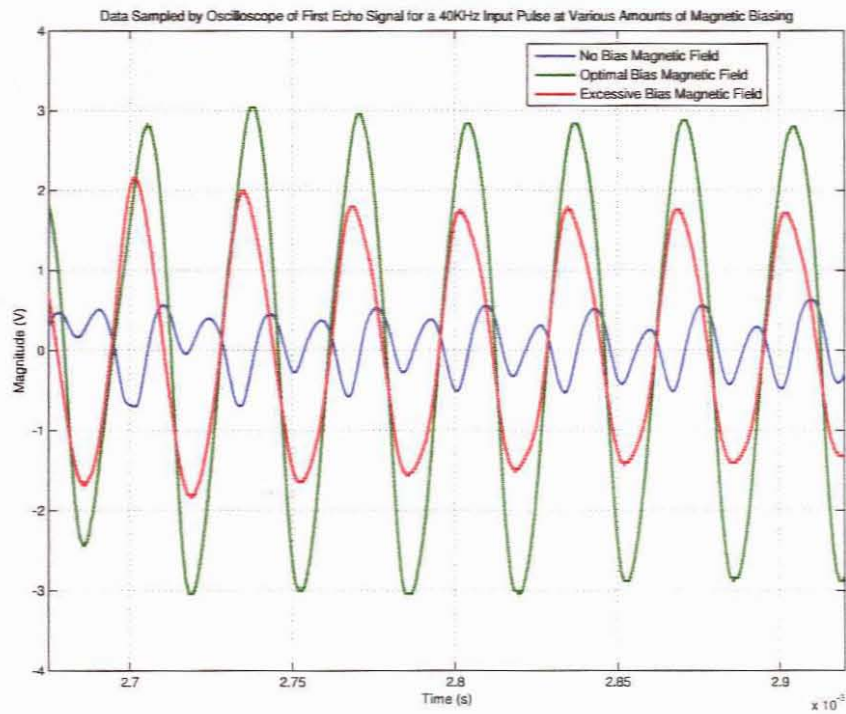
Figure 3.20: The effect magnetic biasing had on the first recovered echo pulse with no magnetic bias, optimal magnetic bias and excessive magnetic bias. Note that for the pulse where no magnetic bias was present, the pulse frequency is doubled

It was found, within the range of the pulse driving circuit, the magnitudes of the recovered echo signals increased linearly with an increase in power to the transceiver coil. Considering Figure 2.8, it was expected that with a further increase in power to the transceiver coil a maximum point of induced strain would be reached during the launch of acoustic pulses. This would cause a fall off in the increase in magnitude of the recovered echo pulses with further increases in power to the transceiver coil. This point could not be reached, because the pulse driving circuit could not supply more power to the transceiver coil. The results of this investigation are shown in Figure 3.22.

3.2.8 The Effect of Applying Tensile Stress to the Waveguide

The magnitude of the first recovered echo pulse was monitored, while tensile stress was applied to the waveguide. This was carried out with the use of the adjusting nut and rod that was connected to the transmission end of the waveguide illustrated in Figure 3.5. The scale also shown in this figure was used to measure the amount of tensile stress that was applied to the waveguide. The driving pulse had a frequency of $40kHz$ and magnitude of $30V_{p-p}$. An optimal bias magnetic field was present. The result of this experiment is shown in Figure 3.23
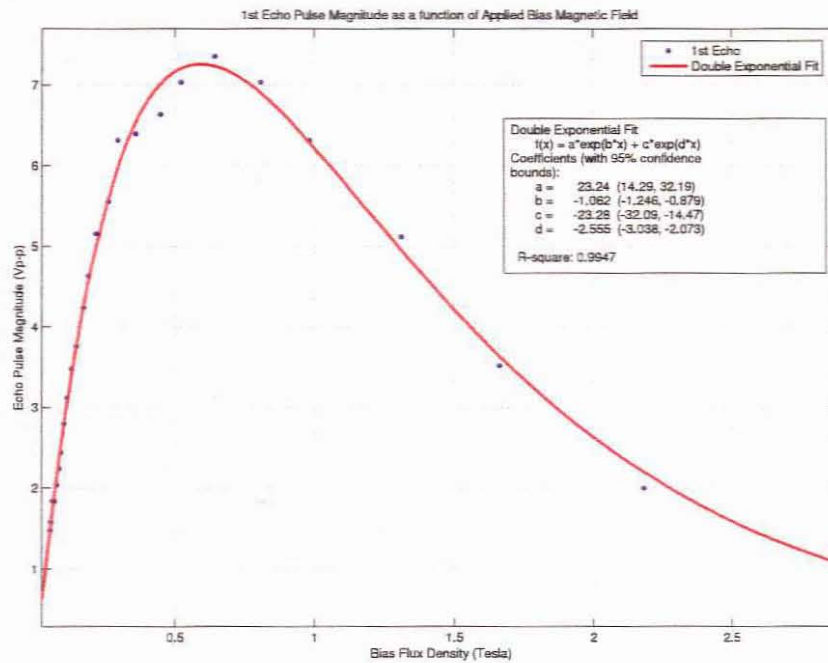
Figure 3.21: The effect of magnetic biasing on the magnitude of the 1st recovered echo pulse fitted with a double exponential equation

It was found the magnitude of the first recovered echo pulse decreased with an increase in the applied tensile stress on the waveguide. The reason for this was the strain produced in the waveguide by the tensile stress and the strain produced by the induced magnetic field in the waveguide during the launch of acoustic pulses was opposite. This caused the amount of negative strain induced during the launch of acoustic pulses with the use of magnetostriction was reduced, which resulted in the launch of acoustic pulses with a decreased magnitude.

3.2.9 The Frequency of the Input Pulse

The frequency of the driving pulse was examined to establish the optimal frequency for the launch of acoustic pulses in the nickel waveguide. The frequency of the input pulse burst was varied while keeping all other input parameters constant. The magnitudes and purity of the signals, as well as the reaction to magnetic biasing was investigated.

The recovered echo signal for a launched pulse frequency of $20kHz$ is shown in Figure 3.24. It was observed the magnitude of the launched echo pulses had increased considerably from the initial results. The presence of unwanted echo pulses was observed. These pulses was substantial in magnitude and repetitive in time, directly following the longitudinal strain pulses. The source of these unwanted pulses could be attributed to the presence of standing waves in the waveguide, or acoustic pulses that had a different mode of propagation. This was investigated

43
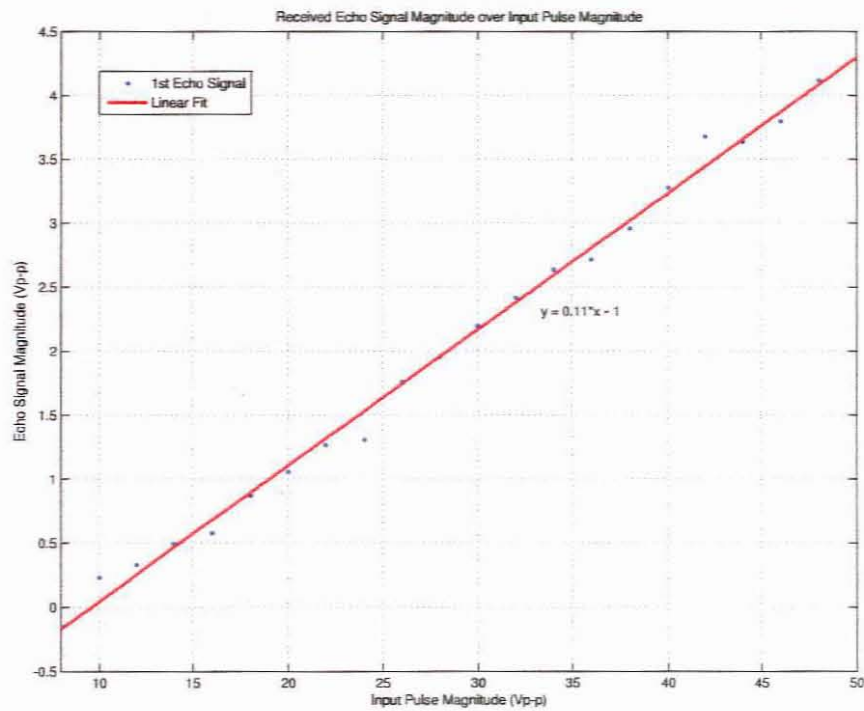
Figure 3.22: The first recovered echo pulse magnitude as a function of driving pulse burst magnitude, fitted with a linear equation

and it was found the unwanted pulses could not be a result of standing waves present in the waveguide, because the length of the waveguide and repetition frequency of the driving pulse burst allowed for the launched pulses to be completely attenuated before the next pulses were launched. The velocity of the unwanted pulses was calculated to establish if they were acoustic pulses with a different mode of propagation. The calculated velocity of the unwanted pulses was $4100ms^{-1}$. The velocity at which shear waves propagate in nickel rods is given by Abramov [1998] as $2960ms^{-1}$, which meant that the unwanted pulses originated elsewhere. Upon further investigation it was found that with an increased driving pulse frequency the magnitude of the unwanted pulses decreased. The recovered echo signals for a driving pulse frequency of $40kHz$ is shown in Figure 3.25. On investigation of the figure a decrease in the magnitude of the unwanted pulses was noted.

It was then speculated the source of the unwanted echo pulses was ringing of the transceiver coil caused by stored electromagnetic force that remained in the transceiver coil after the launch of acoustic pulses was completed. The clipping circuit on the front end of the receive circuit was also suspected of attributing the unwanted echo pulses. It was then decided to investigate the use of separate coils for the launch and recovery of acoustic pulses respectively. It was concluded the optimal driving pulse frequency for the test rig, while using a single coil for the launch and recovery of acoustic pulses, was $40kHz$.

44
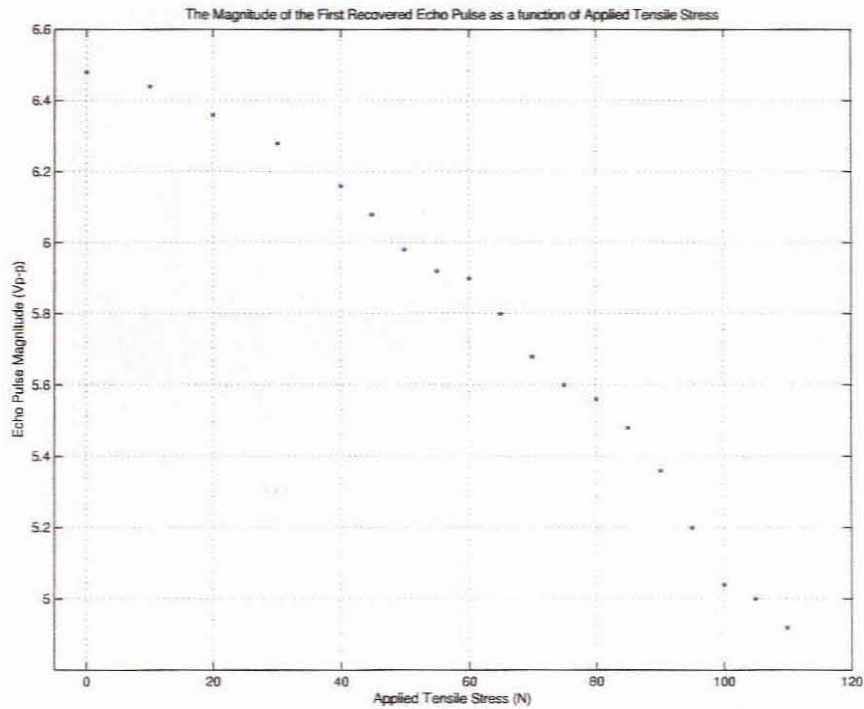
Figure 3.23: The effect of tensile stress applied to the waveguide on the magnitude of the first recovered echo pulse

3.2.10 The Use of Separate Transmit and Receive Coils

The use of separate transmit and receive coils was investigated to in order to establish if the source of the unwanted echo pulses observed in Figure 3.24 and 3.24 was caused by interaction between the pulse generating and receiving hardware. The coils used had the same dimensions as described in Section 3.1.2. The pulse driving circuit was connected over the transmit coil and the receive circuit was connected over the receive coil. The clipping circuit at the front end of the instrumentation amplifier was removed because the voltage across the receive coil would not exceed $15V$. An optimal bias magnetic field, of similar polarity was applied to the waveguide in the region of both coils.

Initially, the correct axial positions of the transmit and receive coils was determined. The correct position of the transmit coil had already been established in section 3.2.2 at $\frac{1}{2}\lambda$. The receive coil was placed at $\frac{1}{4}\lambda$ and $\frac{1}{2}\lambda$ distances from the transmit coil. It was found $\frac{1}{2}\lambda$ was the closest that the receive coil could be placed from the transmit coil before interference took place. The position of the receive coil could be moved further from the transmit coil, as long as it was moved in multiples of $\frac{1}{2}\lambda$. After the optimal coil positions was established, the experiments completed using a single transceiver coil was repeated with separate transmit and receive coils.

45
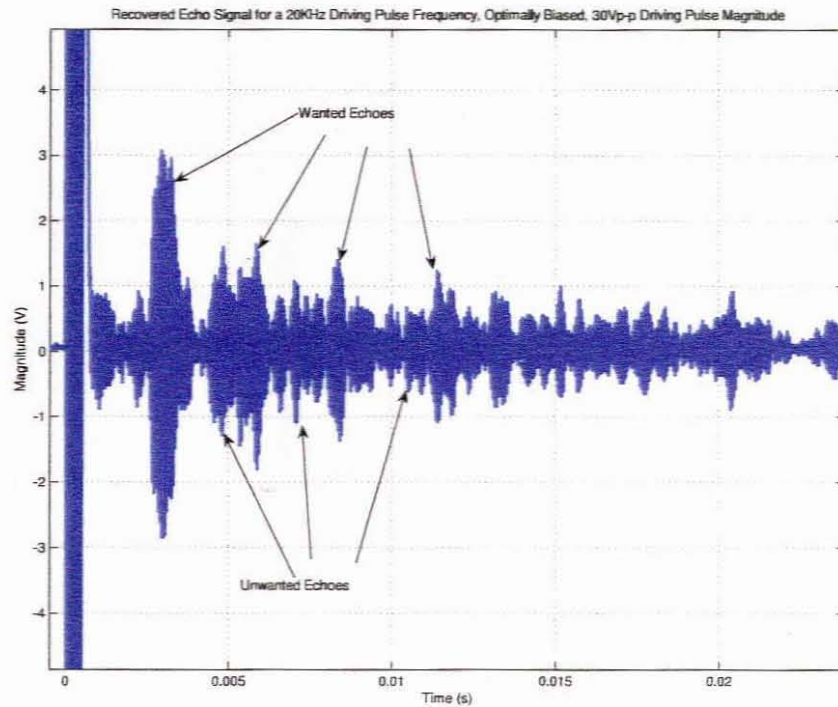
Figure 3.24: The recovered echo signal for a driving pulse frequency of 20kHz. An optimal bias magnetic field was present. Note the presence of unwanted echo pulses.

All the findings made with the single transceiver coil held true for operation with separate transmit and receive coils, although the results found at higher driving pulse frequencies was better. An optimal driving pulse frequency of $60kHz$ was established. The recovered echo signal for a driving pulse frequency of $60kHz$ is shown in Figure 3.26. It was observed the unwanted echo pulses had been dramatically reduced and that the echo pulse magnitude was unaffected. The recovered echo pulses could be clearly identified. It was concluded that the use of separate transmit and receive coils for the launch and recovery of acoustic pulses in the waveguide was optimal for the test rig.

3.3 Summary

A test rig was constructed consisting of a ferromagnetic waveguide, a transceiver coil, and the necessary electronic circuitry for the launch and recovery of longitudinal strain pulses using magnetostriction.

The test rig was used to investigate the behavior of the acoustic pulses and their resultant echoes in the ferromagnetic waveguide. The launch and recovery of the acoustic pulses was optimised through the optimisation of the magnetostrictive effects used during launch and recovery.
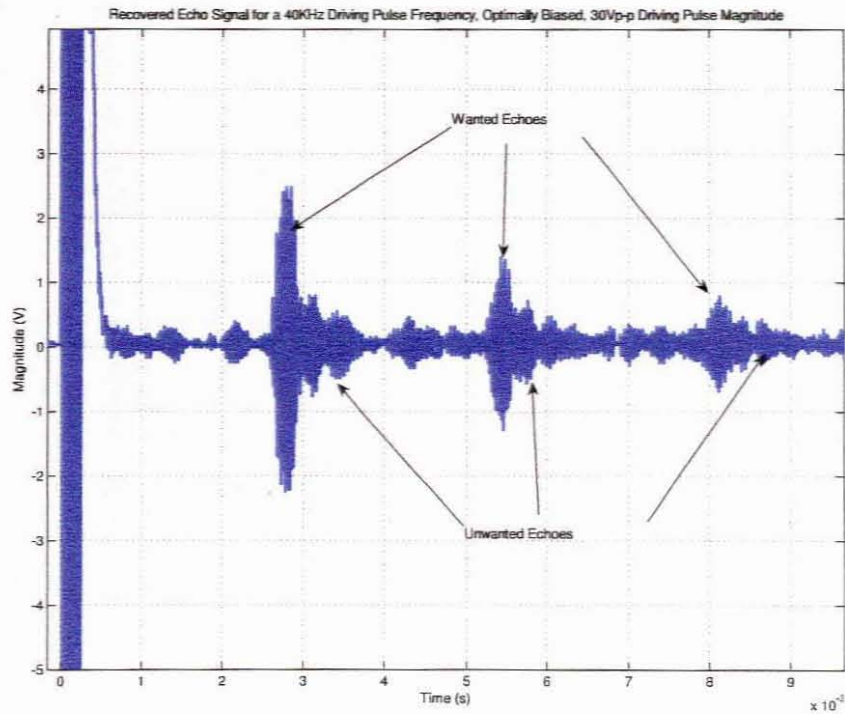
Figure 3.25: The recovered echo signal for a driving pulse frequency of 40kHz. An optimal bias magnetic field was present. The magnitude of the unwanted pulses was decreased with an increase in driving pulse frequency.

This was done with the addition of a bias magnetic field and optimal transceiver coil design for the range of frequencies at which the test rig was investigated. The position of the transceiver coil with respect to the transmission end of the waveguide was important, because interference from echo pulses reflected from the transmission end of the waveguide affected the launched acoustic pulses, during launch and recovery.

Magnetic biasing had the most significant effect on pulse generation and it was found to be critical, both in launch and recovery of acoustic pulses. The addition of a bias magnetic field eliminated the frequency doubling of the launched pulse. The optimal bias magnetic field for the waveguide used in the test rig during experimental work was in the region of $0.63T$. It was found an increase in the power of the driving pulse resulted in a linear increase in the magnitude of the launched acoustic pulses. Applying tensile stress to the waveguide had a negative effect on the generation of acoustic pulses, because it produced an opposite strain in the nickel wire to that produced by the launched strain pulse. This reaction was expected.

On inspection of the optimal frequency for the launch of acoustic pulses, the optimal frequency of the use of a single transceiver coil was found as $40kHz$. There was a significant presence of unwanted echo pulses which was decreased with an increase in frequency. It was decided to investigate the use of separate transmit and receive coils. The use of separate transmit

47
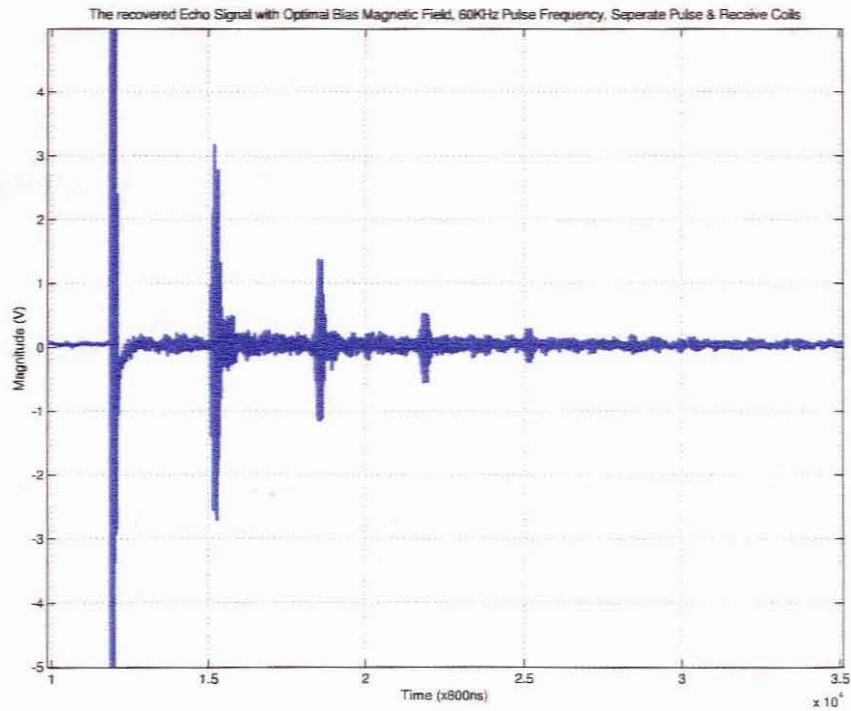
Figure 3.26: The recovered echo signal for a driving pulse frequency of 60kHz and using separate transmit and receive coils. An optimal bias magnetic field was present. The presence of unwanted pulses is minimal.

and receive coils minimised the presence of unwanted echo pulses, and satisfactory results were obtained at higher pulse frequencies. An optimal pulse frequency of $60kHz$ was established. The exact source of the unwanted echo pulses was not established, but they were eliminated with the use of separate transmit and receive coils. The use of separate transmit and receive coils was concluded as the optimal setup for the test rig.

The results obtained through the investigation of the test rig could be used to optimise the design of an acoustic thermometer based on a nickel waveguide using the pulse echo method.

Chapter 4

Design of an Acoustic Thermometer

This chapter focuses on the design of an acoustic thermometer based on a nickel wire waveguide using the pulse-echo method. This type of temperature sensor is ideal for applications in volatile environments, because temperature measurements depend on the propagation of mechanical vibrations through the waveguide material and is non-invasive electronically. This means if the waveguide material is not physically altered by the environment in which the sensor is used, the sensor would be able to function.

4.1 Aim of the Design

The aim of the design was to consolidate the knowledge gained through the optimisation of the pulse echo method and literature review into an application in acoustic thermometry. The designed thermometer had to be optimised and calibrated. The performance of the designed thermometer had to be comparable to that of similar designs by previous researchers. Finally, the accuracy of the instrument had to be established for the range of temperatures from 20^oC to 400^oC.

4.2 Instrument Description

Temperature measurement using the pulse echo method and an acoustic waveguide is based on the temperature dependence of the velocity of sound in the section of the waveguide, referred to as the specimen or probe, that will be subjected to the environment to be measured. In order to measure the velocity of sound in the specimen, a reference echo is required that originates from the start of the probe. This is achieved by creating a point of discontinuity in the waveguide at the point where the probe begins.

The point of discontinuity could be created by coupling a probe of different dimensions, and even a different material than that of the waveguide, to the waveguide as shown by Lynnworth

[1975]. The point of discontinuity could also be created by changing the waveguide itself at the point where the probe begins. This could be done by creating notches in the waveguide as shown by Varela [1984], or by creating a kink in the waveguide as shown by Lynnworth & Spencer [1970].

The point of discontinuity in the waveguide would cause a partial reflection of the propagating acoustic pulse, while the remainder of the pulse continued to propagate through the probe and then reflected from the end of the probe. The echo that was reflected from the point of discontinuity served as a reference echo, signaling the start of the probe. The time delay between the reference echo and the echo reflected from the end of the probe would be equal to twice the time taken for the acoustic pulse to travel the length of the probe.

The instrument designed and the expected signal are shown in Figure 4.1. The waveguide material used was 99.5% pure unannealed nickel wire, $2mm$ in diameter and $3.5m$ in length. The length of the waveguide was decreased from the length used in the test rig in order to decrease the overall size of the instrument.

Separate coils were used for the launch of longitudinal strain pulses and the recovery of resultant echoes. This enabled the movement of the receive coil with respect to the transmission coil and the transmission end of the waveguide in order to manipulate when reflected echoes from the transmission end of the waveguide was received and so doing eliminate interference from unwanted echoes. The use of a separate receive coil allowed for the clipping circuit on the front end of the instrumentation amplifier to be discarded and eliminating the noise that the clipping circuit attributed to the recovered signal. The launch and receive coils had the same dimensions as calculated in Section 3.1.2, and were optimally biased magnetically with rare earth magnets to ensure efficient generation and recovery of acoustic pulses.

The method of creating a point of discontinuity in the waveguide was the same as described by Lynnworth & Spencer [1970], by making a kink in the waveguide at the point where the probe begins. This proved to be the simplest and most successful method of creating a point of discontinuity, because the waveguide was thin and machining or physically altering the waveguide in its diameter would weaken the waveguide at that point. Further advantages in using a kink in the waveguide at the point of discontinuity was that the magnitude of the partially reflected pulse could easily be manipulated by simply changing the angle of the bends in the kink. This proved very important in later experiments.

It was found clutching the waveguide with tongs anywhere along the length of the waveguide caused the entire signal to be reflected from that point. This showed the clutching of a specific area of the waveguide in effect transformed that piece of the waveguide into high impedance termination. The high impedance termination stub at the non-transmission end of the waveguide was removed as it was only soldered onto the waveguide and would lose its coupling to the waveguide at high temperatures.

The signal expected at the receive coil after an acoustic pulse was launched by the transmit coil is shown in Figure 4.1. The first pulse received would be the pulse propagating from

the transmit coil where it was launched. The second expected pulse would be the instance of the launched pulse that propagated to the transmission end of the waveguide and reflected towards the non-transmission end. The first echo pulse expected would be the partial reflection, or reference reflection, from the point of discontinuity at the start of the temperature probe. Finally, the echo pulse reflected from the end of the probe was expected.

The time delay between the arrival of the reference echo and the echo reflected from the end of the probe was used to determine the temperature of the probe section. As the temperature of the nickel changed, the physical properties of the material changed. These properties included the density and the modulus of elasticity, Young's modulus, of the material. The relationship between these physical properties of the material is given in equation 2.40.

The time taken for the longitudinal pulse to travel the length of the probe was obtained by accurately measuring the time delay between the arrival of the reference echo and the echo reflected from the end of the probe. This time delay was divided by two, because the pulse reflected from the end of the probe travels the length of the probe twice. The velocity of the propagating pulse through the probe could be calculated, as the length of the probe was known. The values for the physical properties of the probe material, density and Young's modulus, as a function of temperature were known. The measured pulse velocity for the probe could be directly related to the temperature of the probe material.

Referring to Figure 4.1, the period of the input pulse burst is indicated as T_1, the period of a single pulse in the pulse burst is indicated as T_2, and an indication of the expected echo signal at the receive coil is shown. The time between the reference echo pulse and the echo pulse reflected from the end of the probe is indicated as $2t_{probe}$.

In order to ensure no interference between the reference echo and the echo reflected from the end of the probe, the period of the input pulse burst T_1 had to be small compared the time taken for the end reflected echo signal to propagate through the probe and back, or $2t_{probe}$. This was achieved by making the length of the probe as long as possible. The pulse frequency had to be as high as possible, to decrease the period of the launched pulse. The number of pulses per pulse burst was also minimised, and for two pulses per pulse burst, the period T_1 for a $40kHz$ pulse was:

$$T_1 = 2(\frac{1}{40000})$$
$$= 50\mu s$$

To ensure that the length of the probe section would be sufficient, the time taken for the acoustic pulse to propagate through the probe section twice, $2t_{probe}$, was chosen as $200\mu s$. This gave a calculated probe length of:

52

$$2\ell_{probe} = 2t_{probe} \times c$$
$$\ell_{probe} = t_{probe} \times c$$
$$= 100\mu s \times 4900ms^{-1}$$
$$= 0.49m$$
$$\approx 0.5m$$

The waveguide was supported and held horizontally by the aluminium clamps described in Chapter 3 and acoustically insulated with styrofoam, although the probe section of the waveguide was not held. The wooden platform was used for the electronic circuitry, and the electronic circuitry was the same as used during the investigation of the test rig. The clipping circuit on the front end of the instrumentation amplifier was removed, because it was no longer needed. Data acquisition hardware capable of analog sampling rates of up to 10×10^6 samples per second was connected over the coil. The addition of the data acquisition hardware was to improve the resolution of the signals sampled from the receive coil.

The data acquisition hardware was set up to sample the recovered signal from the receive coil at a rate of 5×10^6 samples per second, and store the data to a file to be processed. To ensure that the readings made by the instrument was consistent, the data acquisition hardware was set up to take 10 sample sets at each measurement interval, triggered externally by the pulse generating hardware to ensure that the data sets were synchronous. Each data set contained 50000 samples, sufficient to sample the entire recovered signal at the selected sample rate.

4.3   Initial Findings and Signal Optimisation

The echo signal received during initial investigation of the instrument is shown in Figure 4.2. It was observed that differentiating between the reference echo and the end reflected echo was difficult to do and that there was still interference present. This was inspected by moving the transmit and receive coils with relation to each other and with relation to the transmission end of the waveguide. It was found the source of the interference was the reflection of both echo signals from the transmission end of the waveguide. This was eliminated by moving the receive coil further away from the transmission end of the waveguide.

The number of pulses per input pulse burst was decreased to a single pulse to decrease the period of the launched acoustic pulse, but the launched pulse consisted of two pulses as it passed the receive coil for the first time. This was also as a result of the reflection of the launch pulse from the transmission end of the waveguide. This occurrence made it difficult to establish the exact position of the reflected echoes in the time domain.

In order to eliminate the reflection of the longitudinal waves from the transmission end of the waveguide, Bell [1957] described an attenuating pad that was in contact with the waveguide
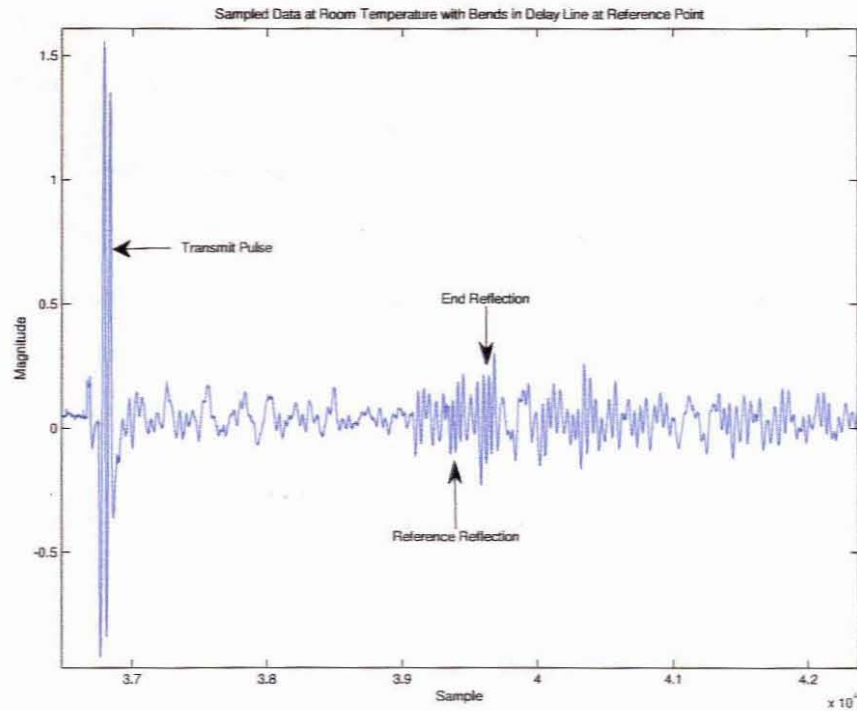
Figure 4.2: Sampled data of initial results obtained by bending the waveguide at the reference point. It can be noted that determining the peaks of the reflected echoes would be difficult because of the presence of unwanted echoes

on the transmission end. The attenuating pad dampened the energy of the acoustic pulses that propagated to the transmission end of the waveguide, thereby eliminating the effects that reflections of these waves had on the returning echoes from the non-transmission end of the waveguide.

The implementation of attenuating pads was not possible for the designed instrument, because it required the length of the instrument be increased and this was not desired. Instead, the high impedance termination stub on the transmission end of the waveguide was removed and the transmit coil was moved to the end of the waveguide. This eliminated the reflection of the launched pulse and ensured only a single acoustic pulse was launched in the waveguide. Moving the transmit coil to the end of the waveguide had a negative effect on the magnitude of the pulse that was launched. The driving power to the pulse coil was increased to the maximum of $50V_{p-p}$ to increase the magnitude of the launched pulse. The receive coil was moved from the transmission end of the waveguide. This was to ensure the reflections of the returning echoes from the transmission end of the waveguide would not interfere with returning echoes. This would occur if the distance between the receive coil and the transmission end was equal to the length of the probe, therefore, the receive coil was moved to a metre from the transmission end of the waveguide.
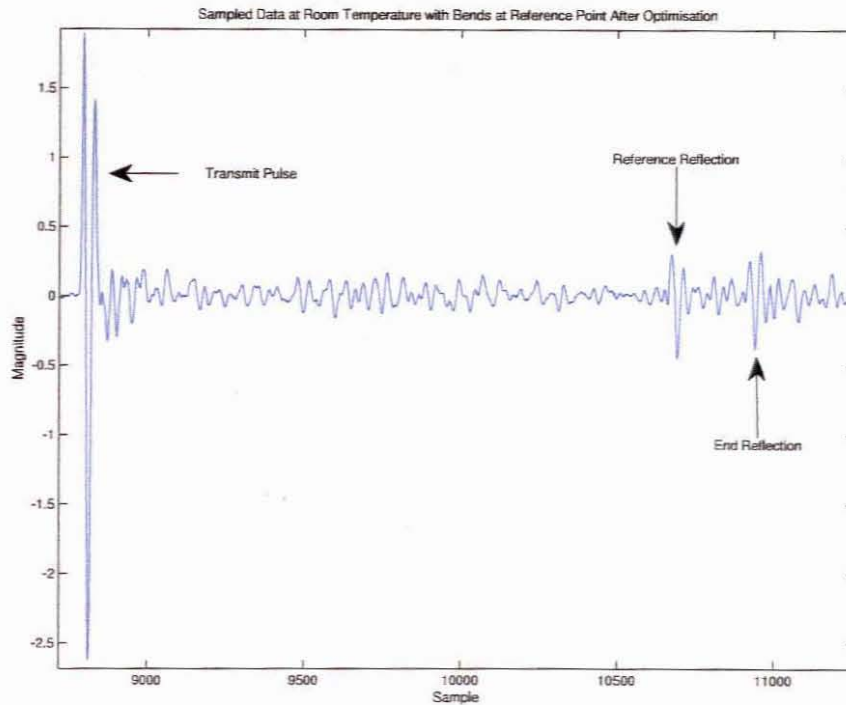
Figure 4.3: Recovered echo signal after improvements to the launch of acoustic pulses was made and the transmit and receive coils were moved to the transmission end of the waveguide and a meter from the transmission end of the waveguide respectively

The echo signal recovered after optimisation of the launched pulse is shown in Figure 4.3. It could be seen that both the reflected echoes consisted of only a single pulse, which made differentiating between the echo signals easier. The period of the launched pulse and resultant echoes could be further reduced by increasing the frequency of the launched pulse and acceptable results were found with pulse frequencies of $80kHz$ and $90kHz$. This is shown in Figure 4.4.

It can also be seen both the reflected echoes had roughly the same magnitude. The angle of both the bends in the kink at this instance was 45°. Changing the angles of the bends in the kink allowed for the control of the magnitudes of both reflected echoes, increasing the bend angles increased the magnitude of the reference reflection and decreased the magnitude of the end reflection. The opposite occurred when the angle of the bends was decreased.

4.4   Signal Processing

Bell [1957] says at high temperatures the magnitude of the end reflected pulse decreased as a result of higher attenuation, although reverberation noise was not affected in the same way. This was found to be true during high temperature measurements made with the instrument. A signal

55
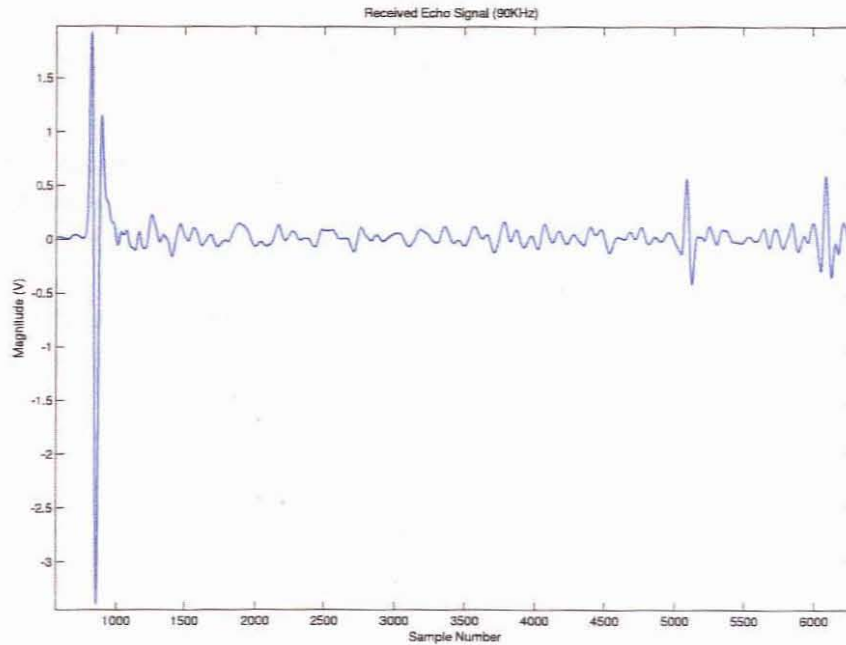
Figure 4.4: Recovered echo signal after improvements and with a launch pulse frequency of 90kHz. Note the decrease in the period of the launched acoustic pulse.

processing method had to be introduced that would be capable of manipulating the received echo signal in such a manner that the transmitted pulse and the resultant echoes be magnified and the unwanted noise eliminated. Furthermore, the signal processing method chosen should not affect the signal in the time domain once applied, to protect the integrity of the measurements. Smith [1997] states that for a signal of known shape, the best way to determine if or where that signal occurred in another signal was through correlation, more specifically cross correlation.

Cross correlation is basically a measure of similarity between two signals as a function of time delay between the two signals. If two continuous signals $f(t)$ and $g(t)$ is considered, the cross correlation of these signals can be expressed mathematically as:

$$(f * g)(t) = \int_{-\infty}^{\infty} \overline{f}(\tau) \; g(t + \tau) \; d\tau \qquad (4.1)$$

where $\overline{f}$ denotes the complex conjugate of f.

This representation changes for discrete signals, and if two discrete signals, $f(n)$ and $g(m)$ is considered, the cross correlation is expressed as:

56

$$(f * g)[n] = \sum_{m=-\infty}^{\infty} \overline{f}[m]\ g[n + m] \qquad (4.2)$$

The data that was sampled after optimisation of the instrument was imported into Matlab. Two sets of data were then created, the first consisting of all the data samples that was imported, labeled $y[n]$, and the second, $x[n]$ consisted of the data samples containing the transmit pulse that first passed through the receive coil. The extracted data samples labeled $x[n]$, is shown in Figure 4.5. The extracted data samples, $x[n]$, was then cross correlated with the data samples $y[n]$, which generated a third set of data, $z[n]$, illustrated in Figure 4.6.
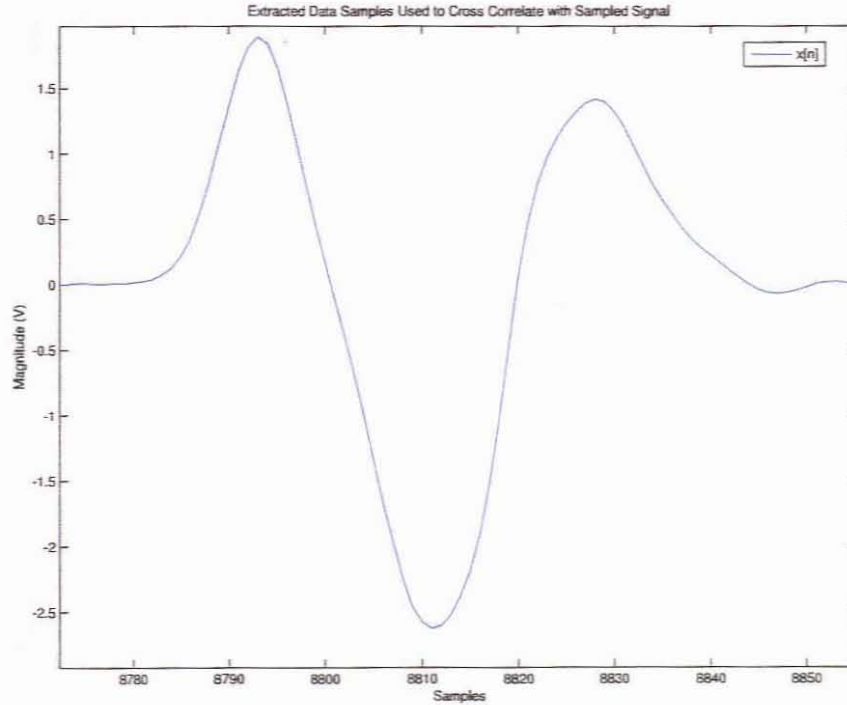
Figure 4.5: The data samples that was extracted from the original signal for cross correlation purposes

Upon investigation of Figure 4.6 it was found the magnitude of both reflected pulses increased quite dramatically. Furthermore, all unwanted noise superimposed on the pulses was eliminated, because the cross correlation data is a representation of the similarity between the initial input pulse and the entire sampled signal, and not the discrete data itself. The peaks that were present in the cross correlation result was a more accurate indication of where the reflected pulses occurred, and the sample difference between the two peaks of the reflected pulses gave a more accurate indication of the time delay between these pulses.
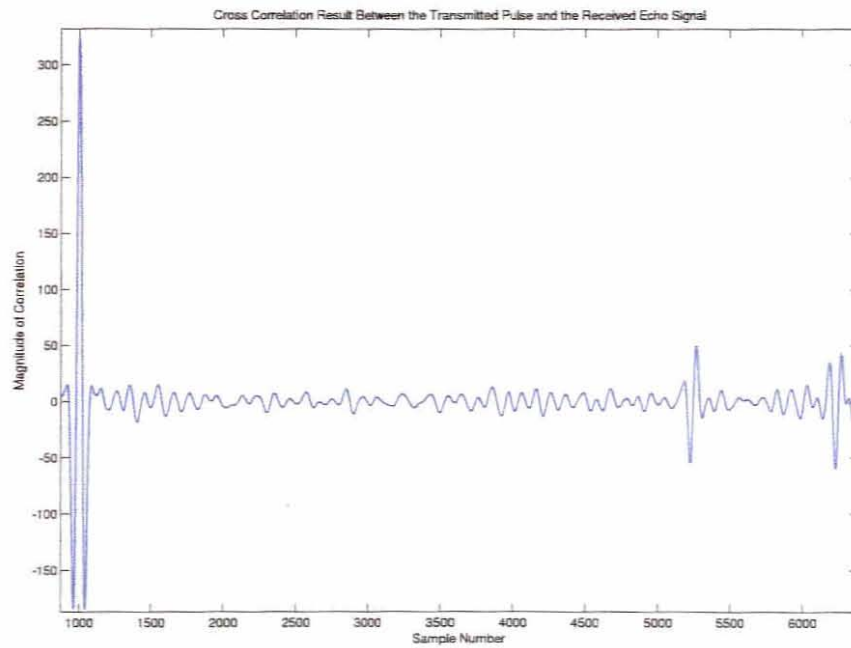
Figure 4.6: The result of cross correlation between the recovered echo signal and the extracted data samples shown in Figure 4.5

4.5 Temperature Measurement

To ensure temperature measurements were reliable and accurate, an isothermal chamber was required to enclose the entire probe. For this purpose a curing oven was used, shown in Figure 4.7. The oven had electronic temperature control that could be preset to the desired temperature and was capable of reaching temperatures exceeding $2000^{o}C$. The oven had a hole in the middle of its door, suitable for inserting the probe. The dimensions of the oven was large enough to completely enclose the probe and ensure constant temperature across the length of the probe.

Figure 4.7: The curing oven with electronic temperature controls used for heat experiments

Temperature measurements were made by setting up the instrument so the probe section was entirely within the curing oven. An accurate definition of the temperature of the oven was established by using a PT1000 temperature probe. The PT1000 temperature probe was placed inside the oven alongside the probe of the instrument through the hole in the door of the oven. The PT1000 temperature probe and the probe of the instrument was insulated from the door of the oven and from each other with thick asbestos rope, which also sealed a hole in the door of the oven and stopped the loss of heat.

Temperature measurements was then made by setting the curing oven to the desired temperature and letting the temperature in the oven stabilise before measurements were made. At each measurement interval the received echo signal was sampled and saved for processing. The temperature range covered in measurements was limited by the PT1000 probe, as the probe was only capable of measuring up to $400^{\circ}C$.

The theoretical values of Young's Modulus and density as a function of temperature for nickel was given referenced to degrees Fahrenheit [Rosenburg, 1968]. Temperature measurements was taken from room temperature, $70^{\circ}F$, at $50^{\circ}F$ intervals up to the maximum value that the PT1000 probe could measure of $750^{\circ}F$. The temperatures corresponding to the measurements was then converted to degrees Celsius for analysis purposes. At each measurement interval the recovered echo signal was sampled by the data acquisition hardware and saved to be processed.

The oven was then switched off and opened to cool down before another set of measurements was done. Three sets of measurements were made. The input parameters to the instrument was kept constant for two of the three sets of measurements, and the frequency of the driving pulse was changed for the third set of measurements. This was to verify the reliability of the measurements, because the velocity at which the longitudinal pulses propagated in the waveguide was independent of the frequency of the acoustic pulse.

4.6   Measurement Results

After the completion of temperature measurements the sampled data was processed. This was done by importing the sampled data sets into Matlab, applying the signal processing method of cross correlation and investigating the result. The exact peaks of the reference echo and the end reflected echo was established. The time delay between the echoes was then calculated.

This was carried out by deducting the peak sample value of the reference reflected echo from the peak sample value of the end reflected echo in the discrete domain. The result was then multiplied by the period at which the echo signal was sampled, in this case $5 \times 10^{-6}s$. This was to convert the data back to the time domain. This process was repeated for all the data sets at each temperature interval and the time delay for each logged. The time delay as a function of temperature for the three sets of measurements is shown in Figure 4.8.

The velocity at which the echoes propagated through the probe, or the velocity of sound in
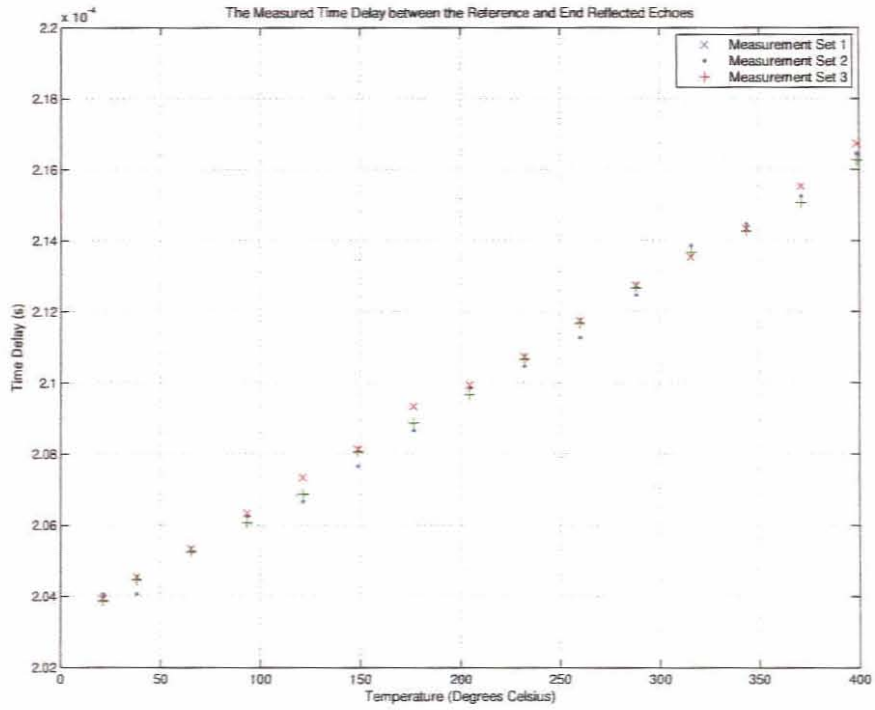
Figure 4.8: The time delay between the reference echo and the end reflected echo as a function of temperature for three sets of measurements

the probe, could be calculated with the following equation:

$$c = \frac{d}{t} \qquad (4.3)$$

where d is the distance propagated, or twice the length of the probe ℓ_{probe} and t is the time delay. The exact length of the probe was required for this calculation, because a difference of $1mm$ in the length equates to a difference of $5ms^{-1}$ in calculation. The length of the probe was measured as $490mm$. The measured values of sound velocity as a function of temperature for the three sets of measurements is shown in Figure 4.9.

4.7 Summary

An acoustic thermometer based on a ferromagnetic waveguide and using the pulse echo method was designed. A discontinuity was created by making a kink in the waveguide, defining a probe section at the end of the waveguide. The kink caused a portion of the propagating acoustic
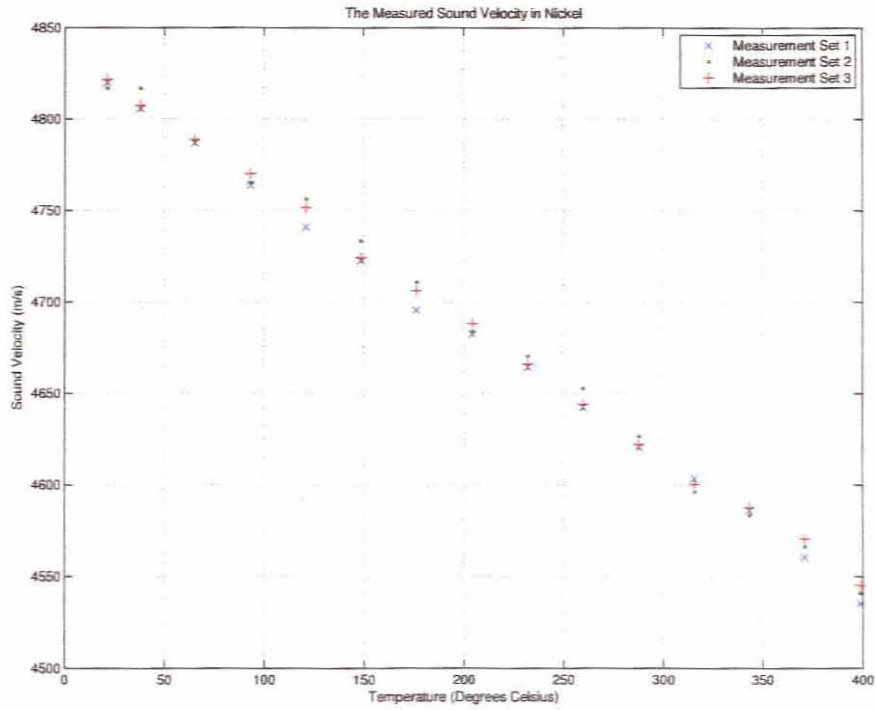
Figure 4.9: The measured velocity of sound in Nickel as a function of temperature for three sets of measurements

pulse, launched with the use of a copper coil wound over the waveguide and magnetostriction, to be reflected from the point of discontinuity. This reflection was used as a reference echo signal.

The time delay between the arrival of the reference echo and the echo reflected from the end of the probe was used to calculate the velocity of sound in the waveguide material as a function of temperature. It was found that the velocity of sound in nickel decreased linearly with an increase in temperature. The results obtained from temperature measurements could now be analysed and the accuracy of the instrument could be determined.

61

Chapter 5

Analysis of Results

In this chapter the results obtained from temperature measurements with the designed acoustic thermometer are analysed. This is achieved by considering both the random and systematic errors that could affect the performance of the instrument. The analysed results are then compared to the expected results referenced for the velocity of sound in nickel as a function of temperature to establish the accuracy of the instrument.

5.1 Analysis of Measured Results

Errors that occur during experimental measurements can be divided into two categories - random and systematic. Random errors affects each measurement differently, and can be established by repeating the same measurement several times. Systematic errors affect each measurement in an identical manner. Systematic errors must be determined and compensated for before measurements are made.

An example of a random error relating to the acoustic thermometer could be that the measurement was not taken at the exact temperature interval as intended. In the case of systematic errors, an example was that the PT1000 probe used to reference the exact temperature of the oven had a consistent measurement error. This error propagated through all measurements made with the instrument, and affected each measurement similarly.

To establish the total error and accuracy of the acoustic thermometer, both the random error and systematic error has to be calculated and combined. The true value for the velocity of sound in nickel must be evaluated from the measured results. This is mathematically represented by Taylor [1997]:

$$c_{true} = c_{mean} \pm \delta c \tag{5.1}$$

62

where c_{mean} is the average measured value for the velocity of sound in nickel at a specified measurement interval and δc is the total error. The total error is given mathematically as:

$$\delta c = \sqrt{(\delta c_{ran})^2 + (\delta c_{sys})^2}$$

(5.2)

where δc_{ran} and δc_{sys} are the random error and systematic error respectively.

5.1.1 Systematic Errors

Systematic errors were known prior to making measurements and affected all measurements equally. They include the error in the reference temperature measurement made with the PT1000 probe, establishing the exact length of the probe section of the waveguide and the occurrence of a double pulse reflection a the kink in the waveguide. The maximum error of the PT1000 probe was specified as 0.25% Early [1982]. The length of the probe was measured using a tape measure. The error of the tape measure was specified as 0.1%.
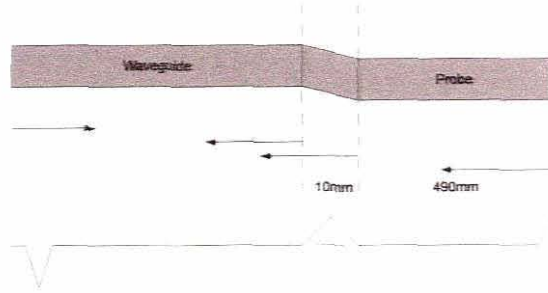
Figure 5.1: An illustration of the kink in the waveguide used to define the probe. The dotted lines indicate where boundary conditions exists and reflections will take place. At the kink, a double reflection takes place, causing the two pulses reflecting from the kink to be superpositioned

To calculate the total systematic error component, all systematic errors must be summed in quadrature. If one denotes the systematic error attributed by the PT1000 probe as δT_{sys} and the systematic error attributed by the wrongful measurement of the length of the probe section as $\delta \ell_{probe}$, the total systematic error can be calculated by:

$$\delta c_{sys} = c_{mean} \times \sqrt{(\frac{\delta T_{sys}}{T})^2 + (\frac{\delta \ell_{probe}}{\ell_{probe}})^2}$$

(5.3)

The systematic error component of the measured results was calculated as 0.27%.

A systematic error was also introduced by the kink in the waveguide. The kink and its dimensions are illustrated in Figure 5.1. A double reflection of the propagating pulse took place at the kink, and because the lenth of the kink section is only $10mm$, the double reflected pulses were superpositioned. To establish the systematic effect that the superpositioning of the double reflection at the kink had, the time delay between the two reflections had to be established. This was effected by calculating twice the time it would take the pulse to propagate the length of the kink section, and for a $90kHz$ pulse this time delay was calculated as $3.47\mu s$. The launched pulse was extracted from a set of sampled data in Matlab and superpositioned with the same pulse, shifted by the calculated time delay. The result is illustrated in Figure 5.2.
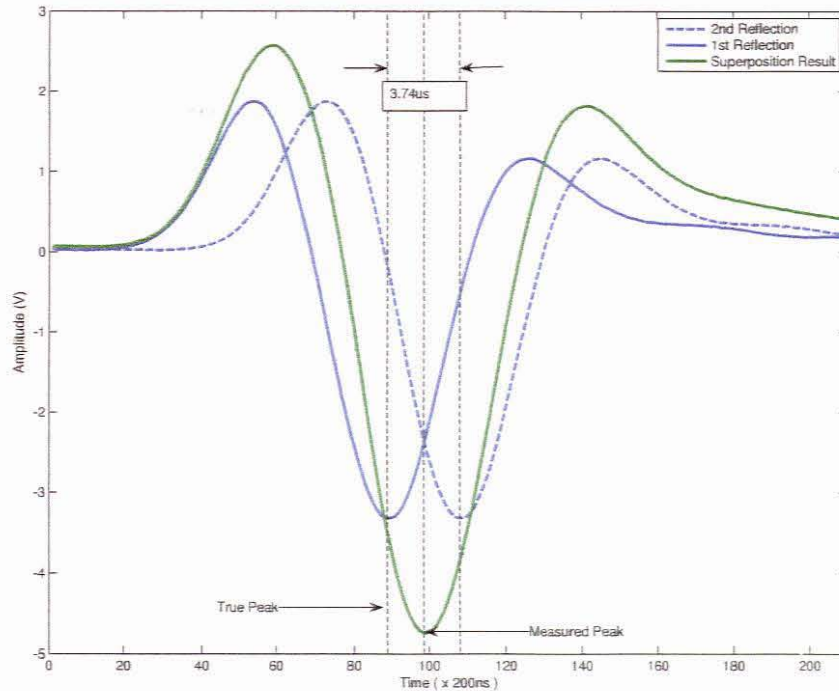
Figure 5.2: Two instances of the same pulse, shifted by a time delay and superpositioned. The true peak and the measured peak is indicated

It can be seen from Figure 5.2 the measured peak was delayed in time. The time delay between the true pulse and the measured pulse was found to be half of the time delay between the two superpositioned pulses. This was because the magnitude of both pulses used during analysis was the same. This would not occur during the double reflection at the kink, because the delayed reflection would suffer attenuation while propagating the length of the kink and during reflection. If the delayed reflection had a smaller magnitude than that of the true reflection, the superpositioned peak would move closer to the true peak. Because the kink section was small in comparison with the length of the waveguide, the losses suffered by the delayed reflection was neglected. The systematic effect contributed by the double reflection at the kink section was a $1.74\mu s$ delay in the detection of the true peak of the reference reflection. This in turn

64

related to a decrease in the measured time delay between the reference and end reflected echoes of $1.74\mu s$. This increase in time delay was added to the measured results as a calibrating factor after measurements were completed.

It was noted by superpositioning of the double reflected pulses the resultant peak was amplified. The pulse used during this analysis was an instance of the launched pulse. The reflected pulses would have been phase shifted by 180°, as can be seen in Figure 4.6. It was also noted that the prominent shoulder of the launched pulse was amplified more as a result of superposition. This served as an explanation for the deformation the reference reflected pulse suffered.

5.1.2 Random Errors

To calculate the random error component, δc_{ran}, for a measurement interval, the measurement must be repeated to obtain a series of identical measurements. This series of values can be expressed as $c_1, c_2, ..., c_N$. The mean $\bar{c}$ of these values must then be calculated by:

$$\bar{c} = \frac{c_1 + c_2 + ... + c_N}{N} \qquad (5.4)$$

Once the mean is calculated for a measurement set, the deviation d of each of the measurements from the mean value is calculated by subtracting the mean value from each of the measured values, or:

$$d_i = c_i - \bar{c} \qquad (5.5)$$

The variance can now be calculated by dividing the sum of the squares of the deviations with the number of measurements minus one, given as:

$$Variance = \frac{\sum_{i=1}^{N}(d_i)^2}{N-1} \qquad (5.6)$$

From the variance, the standard deviation, SD_c, can be calculated by taking the square root of the variance:

$$SD_c = \sqrt{\frac{\sum_{i=1}^{N}(d_i)^2}{N-1}} \qquad (5.7)$$

The standard deviation can now be used to calculate the standard deviation of the mean, $SD_{\bar{c}}$, or the random error component δc_{ran}:

$$SD_{\bar{c}} = \delta c_{ran} = \frac{SD_c}{\sqrt{N}} \tag{5.8}$$

The calculated random error for the measured values of sound velocity was highest for the measurements made at 150^oC at 0.07%. This value was used as the random error component for all measurement intervals in the range.

5.1.3 Total Error

The total error for the measured results was calculated as 0.28% using equation 5.2. This related to a highest error margin of $13ms^{-1}$ at 20^oC. This value was used as the error margin during comparison with the referenced values.

5.2 Comparison between Referenced and Measured Results

The values for the density of nickel as a function of temperature was obtained from reference, where it was specified that the error in the values of density is 10% [ASME, 2007]. The values for Young's Modulus as a function of temperature was referenced from three sources [Rosenburg, 1968] [ASME, 2007] [ThyssenKrupp VDM, 2002]. None of these references specified an error margin in their values, although two of these references are regarded as accepted standards [Rosenburg, 1968] [ASME, 2007]. The mean of the three referenced values was calculated and is illustrated in Figure 5.3. It could be seen that there was discrepencies between the referenced values of Young's Modulus. The standard deviation of the mean for the referenced values of Young's Modulus was calculated as 0.34%. The mean values for Young's Modulus was used in comparison with the measured results.

The referenced velocity of sound in nickel as a function of temperature was calculated using the mean values of Young's Modulus and equation 2.40. This result is illustrated in Figure 5.4 along with the values of sound velocity measured with the designed instrument. The measured results was fitted with an error bar of $13ms^{-1}$, as was calculated during error analysis. The error in the referenced velocity of sound was calculated as 5% using equation 5.9.

$$\frac{\delta c_{ref}}{c} = \frac{1}{2}\sqrt{(\frac{\delta Y_0}{Y_0})^2 + (\frac{\delta \rho}{\rho})^2} \tag{5.9}$$

The average discrepancy between the measured and the calculated referenced values of sound
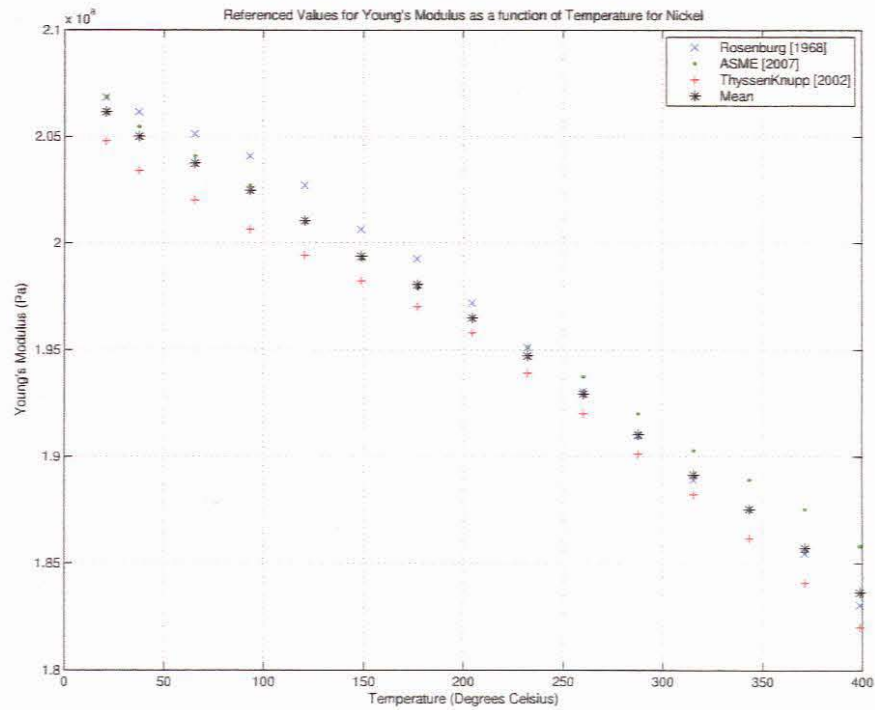
Figure 5.3: The referenced values of Young's modulus as a function of temperature and the mean of these values. The mean values were used during the further calculations and comparison with measured results

velocity as a function of temperature was calculated as $4.43ms^{-1}$. The maximum discrepancy was $6.75ms^{-1}$. This related to a maximum discrepancy of 0.14%.

The measured result for the sound velocity in nickel as a function of temperature is illustrated in Figure 5.5. The result was fitted with a linear polynomial to establish a mathematical represention. The correlation coefficient of the linear fit is 0.9995. This gives the linear equation for the measured result with error as:

$$c_{measured} = (-0.737T + 4873) \pm 0.14\%$$

(5.10)

If the error of the measured result is used, the accuracy of the designed thermometer was $\pm 0.56^{o}C$ over the range of $20^{o}C$ to $400^{o}C$.
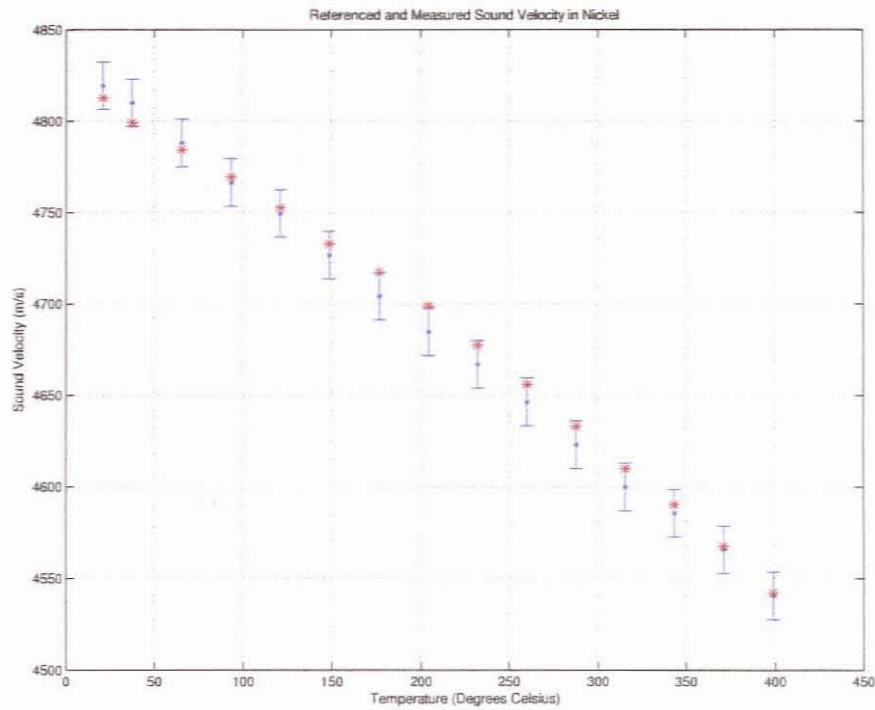
Figure 5.4: The calculated and measured velocity of sound in nickel as a function of temperature. The measured values are fitted with error bars

5.3 Summary

The results obtained from temperature measurements using the designed acoustic thermometer were analysed. This was done by considering both the random errors and systematic errors that affected the measurements made with the instrument. A comparison was made between the analysed measured result and the expected result obtained from referenced values. It was clear that the measured values corresponded with referenced values and that the discrepancies between the values fell within the acceptable limits calculated from error analysis. The accuracy of the designed acoustic thermometer was also established. The results could now be discussed and conclusions drawn.
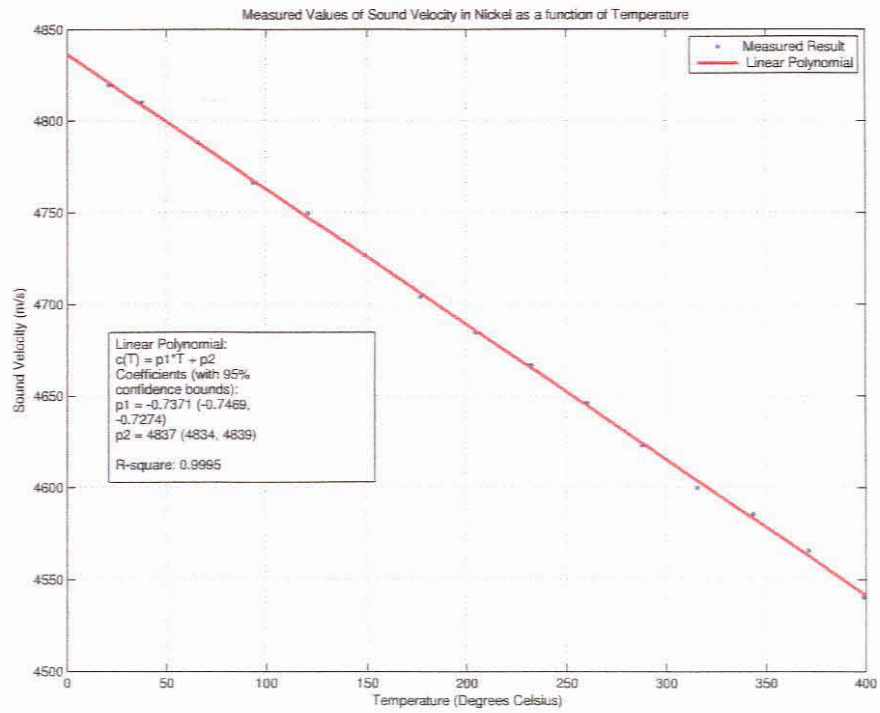
Figure 5.5: The measured values of sound velocity fitted with a linear polynomial. The least square regression coefficient was 0.9995

Chapter 6

Discussion and Conclusions

In this chapter the results obtained from the optimisation of the pulse echo method and the design of an acoustic thermometer are discussed. The chapter will then conclude this thesis and make recommendations.

6.1 Discussion

It was found the most significant contribution to the launch of acoustic pulses was the addition of a bias magnetic field to the region where wave generation took place in the waveguide. The correct positioning of the transceiver coil with respect to the transmission end of the waveguide was important, as the reflection of the launched pulse from the transmission end of the waveguide would interfere with the launched pulse. The axial placement of the transceiver coil was dependant on the termination of the waveguide at the transmission end. The transceiver coil used was designed to induce sufficient magnetic field into the waveguide material for the frequency bandwidth investigated. The inner diameter of the transceiver coil was small in order to be as close to the waveguide as possible. This was done to ensure optimal transduction of magnetic field.

The hardware that was designed for the excitation of the transceiver coil had the ability to generate pulses with variable frequency, variable pulse repetition frequency and variable magnitude. The number of pulses generated per pulse burst was also variable. This enabled a thorough investigation of the launched acoustic pulses and the quantification of the optimal pulse attributes for the waveguide used. The magnitude of the launched acoustic pulses increased with an increase in power in the driving pulse sent to the transceiver coil. A driving pulse frequency of $30kHz$ was found to be the optimal frequency for signal generation during investigation of the test rig with the use of a transceiver coil. Using separate transmit and receive coils gave better results and eliminated unwanted noise in the received signal. The optimal pulse frequency using separate transmit and receiver coils were $60kHz$. This frequency was revised during the design of an acoustic thermometer, and it was found that $90kHz$ was more suited. The reason for this was the reduction in the period of the pulse.

The ferromagnetic waveguide used during initial experiments had a length in excess of $5m$, to clearly observe the propagation of acoustic pulses. The launched acoustic pulses had a longitudinal mode of propagation, although torsional pulses were also observed. The magnitude of the launched acoustic pulses were influenced negatively with the application of tensile stress to the waveguide. This reaction was expected, because the direction of the tensile stress and the strain induced by the transceiver coil during signal generation was opposite.

An acoustic thermometer was then designed by altering the waveguide used in the test rig. A probe section was defined at the non-transmission end by making a kink in the waveguide. Temperature measurements could then be made by measuring the time delay between echoes reflected from the kink in the waveguide and the non-transmission end of the waveguide. It was observed from the results obtained through measurements that the velocity of sound in the probe decreased with an increase in temperature. An error analysis of the measured results showed an error margin in measured results of 0.28% due to both random and systematic errors.

In comparison with the expected results obtained from references the measured results showed a close relation. The gradient at which the velocity of sound decreased in measurement and from reference was the same, and the discrepancies between the measured values and referenced values across the entire range of measurements was within the acceptable limits established through error analysis.

The sample frequency of the data acquisition hardware was 5×10^6 samples per second, giving a sample period of $200ns$, which is 10 times smaller than the time resolution obtained by Mi *et al.* [2003]. In comparison with the results obtained by Bell for an unannealed nickel specimen, shown in figure 2.10 it was observed that the values Bell obtained for sound velocity were higher and that the decrease in sound velocity with an increase in temperature was less linear. A speculation for the reason of the higher sound velocities could be as a result of using a thicker diameter probe. Yamamoto [1951] showed an increase in Young's Modulus in nickel when the angle in the mode of propagation deviated from 90°, reaching a peak value of approximately $250GPa$ at 50°. This would give a calculated sound velocity in nickel of approximately $5300ms^{-1}$. Bell found a sound velocity in unannealed nickel at room temperature of almost $5000ms^{-1}$, which gives a Young's modulus of $220GPa$, relating to a 75° angle possible in mode of propagation from Yamamoto's results.

Lynnworth specified the resolution of a quartz thermometer, an acoustic thermometer using the resonant method, as 0.1 millidegree over the range of -80^oC to 250^oC. Bell's result of $\pm 2^oC$, measuring up to 2000^oC related to a 0.1% error margin [Fathimani & Bell, 1978]. The accuracy of the designed instrument was established as $\pm 0.56^oC$ over the range of 20^oC to 400^oC, which would be comparable to that of Bell's.

The error margin in measurements could be decreased with proper calibration of the instrument in a controlled environment. This would decrease the systematic error component dramatically. The accuracy of the instrument would then depend on the elimination of random errors and the frequency at which the recovered echo signals was sampled.

6.2 Conclusions

The pulse echo method for sensing applications based on ferromagnetic waveguides and using magnetostriction to launch and recover acoustic pulses was optimised. This was achieved by optimising the magnetostrictive effects used during acoustic pulse generation and recovery. A study of magnetostriction and its effects for the use of longitudinal acoustic wave generation in a ferromagnetic waveguide was completed. A study of the ferromagnetic material nickel and its magnetic and elastic properties was completed. A test rig was constructed and the necessary electronic circuitry was designed that enabled a thorough investigation of acoustic pulse generation, recovery and behavior in a ferromagnetic waveguide. The factors that had an influence on the generation, recovery and behavior of acoustic pulses in a ferromagnetic waveguide was quantified, making reproduction of the results possible.

The knowledge gained through literature review and the investigation of a test rig was consolidated in the design of an acoustic thermometer. The acoustic thermometer was based on a ferromagnetic waveguide and used the pulse echo method for measurements. It was shown that by measuring the velocity at which an acoustic pulse propagates through a section of a ferromagnetic waveguide the temperature of that section could be established. The implementation of powerful data acquisition hardware in the sampling of recovered echo signals improved the accuracy of the instrument. The use of powerful data acquisition hardware and by applying the cross correlation signal processing method to sampled signals the time resolution of the instrument was increased and the peaks of the recovered pulses were magnified.

The designed acoustic thermometer showed a close relation in performance to the expected results obtained from reference. In comparison with the expected referenced results the results obtained with the instrument fell within the acceptable limits for discrepancies. In comparison with the results obtained by previous researchers the performance of the designed instrument was acceptable, considering that the results was obtained in a non-controlled environment. The accuracy of the instrument was established and defined.

6.3 Recommendations and Future Work

Although satisfactory results were obtained with the designed acoustic thermometer there are still a number of improvements that will increase the accuracy of the instrument. The following recommendations will assist in future improvements:

- The electronic circuitry designed for the generation of longitudinal strain pulses and the recovery of the resultant echoes was susceptible to noise from ground interference. The reason for this was that the ground reference was switched during signal generation and during signal recovery there was no ground reference, as the signals were differential. Although this did not affect the measurements made during test rig investigation or temperature measurements, it would be advisable to improve this hardware before commercial

implementation of the instrument;

- the wound copper coils used to generate and detect the magnetic field effects of magnetostriction was designed to function over the range of frequencies that was investigated, and not for a specific operational frequency. Designing coils for a specific frequency of operation will improve the performance of the instrument;

- the performance of any instrument that implements the pulse echo method and a ferromagnetic waveguide depends greatly on the properties of the ferromagnetic material used for the waveguide. The correct selection of material for the purpose of the instrument is, therefore, critical. For the use of temperature measurement, and especially the probe section, materials such as sapphire and graphite can also be investigated;

- The presence of unwanted echo reflections in the waveguide can be eliminated with the implementation of attenuating pads;

- and calibration of the instrument in a controlled environment will decrease the error margin in measurements and, therefore, the accuracy of the instrument.

References

Abramov, O.V., 1998, *High-Intensity Ultrasonics: Theory and Industrial Application*, Gordon and Breach Science Publishers.

ASME, 2007, *ASME Boiler and Pressure Vessel Code*, The American Society of Mechanical Engineers.

Bell, J.F.W., 1957, *The velocity of sound in metals at high temperatures*, The Philosophical Magazine, 2:1113–1120.

Bell, J.F.W., 1972, *Acoustic thermometers*, United States Patent 3633423.

Bell, J.F.W. & Mosby, E.G.H., 1970, *Acoustical thermometry*, United States Patent 3487690.

Bird, J., 2003, *Electrical and Electronic Principles and Technology*, 2nd edition, Newnes.

Coulter, J.D., 1987, *Phenomena in the Propagation of Ultrasonic Vibrations in Nickel Wire*, Master's thesis, University of Cape Town.

Crawford, A.E., 1955, *Ultrasonic Engineering*, Butterworths Scientific Publications.

Early, B., 1982, *Temperature Sensing with Thermocouples and Resistance Thermometers*, 2nd edition, Labfacility Ltd.

Fathimani, A.A. & Bell, J.F.W., 1978, *A new resonant thermometer for nuclear reactor applications*, Journal of Physics E: Scientific Instruments, 11:588 – 596.

Glover, G.M., Hall, G., Matheson, A.J., & Stretton, J.L., 1968, *A magnetostrictive instrument for measuring the viscoelastic properties of liquids in the frequency range 20-100KHz*, Journal of Physics E: Scientific Instruments, 1:383–388.

Gooberman, G.L., 1969, *Ultrasonics: Theory and Application*, Hart Publishing Company Inc. New York, NY.

Heuter, T.F. & Bolt, R.H., 1955, *Sonics*, John Wiley & Sons, Inc.

Hristoforou, E., 2002, *Amorphous magnetostrictive wires used in delay lines for sensing applications*, Journal of Magnetism and Magnetic Materials, 249:387–392.

Hristoforou, E., 2003, *Magnetosrtictive delay lines: engineering theory and sensing applications*, Measurement Science and Technology, 14:R15–R47.

Hristoforou, E., Hauser, H., & Niarchos, D., 2002, *Magnetostrictive delay line characterisation*, Journal of Magnetism and Magnetic Materials, 242-245:269–272.

Jiles, D., 1991, *Introduction to Magnetism and Magnetic Materials*, Chapman & Hall.

Karagiannis, V., Manassis, C., & Bargiotas, D., 2003, *Position sensor based on the delay line principle*, Sensors and Actuators A, 106:183–186.

Kim, J.O. & Bau, H.H., 1989a, *Instrument for simultanious measurement of density and viscosity*, Review of Scientific Instruments, 60:1111–1115.

Kim, J.O. & Bau, H.H., 1989b, *On line, real-time densimeter - theory and optimization*, Journal of the Acoustic Society of America, 85:432–439.

Kinsler, L.E. & Frey, A.R., 1950, *Fundamentals of Acoustics*, John Wiley & Sons, Inc.

Kraus, J.D. & Carver, K.R., 1973, *Electromagnetics*, 2nd edition, McGraw-Hill.

Kwun, H. & Bartels, K.A., 1998, *Magnetostrictive sensor technology and its applications*, Ultrasonics, 36:171–178.

Lynnworth, L.C., 1970, *Dual ultrasonic sensors employing differing modes of ultrasonic transmission*, United States Patent 3540265.

Lynnworth, L.C., 1977, *Slow torsional wave sensors*, Proceedings of the IEEE Ultrasonics Symposium, 1:29–34.

Lynnworth, L.C., Carnevale, E.H., & Claidman, S.L., 1965, *Ultrasonic temperature measuring device*, Technical report, Panametrics Inc.

Lynnworth, L.C. & Spencer, B.J., 1970, *Ultrasonic sensing system*, United States Patent 3514747.

Lynnworth, L., 1975, *Industrial applications of ultrasound - a review ii. measurements, tests and process control using low intensity ultrasound*, IEEE Transactions on Sonics and Ultrasonics, SU-22:71–101.

Mi, X.B., Zhang, S.Y., Zhang, J.J., & Yang, Y.T., 2003, *Automatic ultrasonic thermometry*, Proceedings of the 15th Symposium on Thermophysical Propetries, Boulder, Colorado, USA.

Rosenburg, S.J., 1968, *Monograph 106: Nickel and its Alloys*, Institute for Materials Research, National Bureau of Standards.

Smith, S.W., 1997, *The Scientist and Engineers Guide to Digital Signal Processing*, California Technical Publishing.

Tasman, H.A. & Patzold, E.E.S., 1980, *Ultrasonic thermometer*, United States Patent 4195523.

Taylor, J.R., 1997, *An Introduction to Error Analysis*, 2nd edition, University Science Books.

Thompson, R.B., 1978, *A model for the electromagnetic generation of ultrasonic guided waves in ferromagnetic metal polychrystals*, IEEE Transactions on Sonics and Ultrasonics, SU-25:7–15.

ThyssenKrupp VDM, 2002, *Nickel 99.2 - Alloy 200 & Nickel 99.2 - Alloy 201: Material Data Sheet 1001*, ThyssenKrupp VDM.

Tzannes, N.S., 1966, *Joule and Wiedemann effects - The simultanious generation of longitudinal and torsional stress pulses in magnetostrictive materials*, IEEE Transactions on Sonics and Ultrasonics, SU-13:33–41.

Varela, D.W., 1984, *Ultrasonic thermometer*, United States Patent 4483630.

Yamamoto, M., 1951, *Elastic constants of nickel crystals*, Technical Report 634, The Research Institute for Iron, Steel and other Metals.
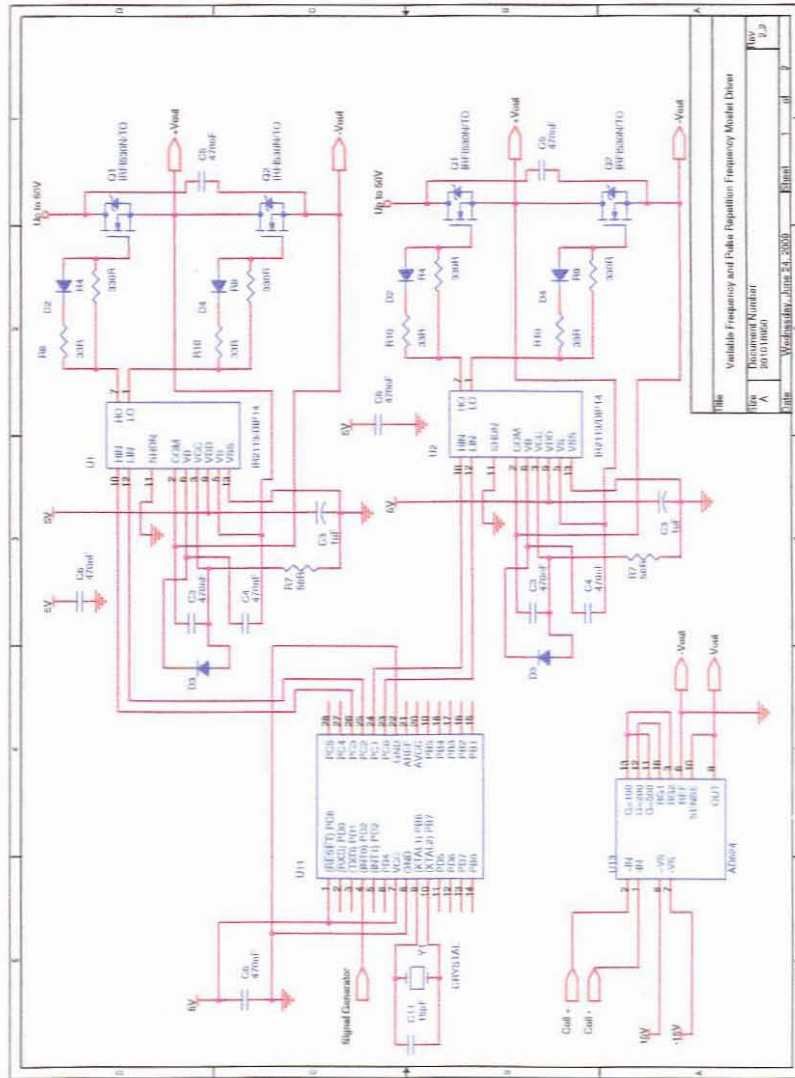
Figure A.1: The schematic diagram of the hardware used to generate the pulses and drive the transceiver coil.

Appendix B

Embedded Source Code

```
/******************************************************
 * Full Bridge MOSFET Driver Pulse Generator
 *
 * G.C. Burger
 ******************************************************/

#include <C:\mosfetdriver\INC\io.h>
#include <C:\mosfetdriver\INC\iom8.h>
#include <C:\mosfetdriver\INC\delay.h>
#include <C:\mosfetdriver\INC\signal.h>
#include <C:\mosfetdriver\INC\interrupt.h>
#include <C:\mosfetdriver\INC\inttypes.h>

unsigned int pcount;
unsigned int dcount;
unsigned char out;

int init(void)
{
        pcount = 0x00;
        dcount = 0xBB8;
        out = 0x00;
        PORTC = out;
        DDRC = 0xFF;
        DDRD = 0x00;
        GIMSK = (1<<INT0);
        GICR = 0x40;
        MCUCR = 0x0D;

        sei();

        return(0);
}

int main (void)
{
        init();

        while(1)
        {
        }
}
```

```
INTERRUPT(SIG_INTERRUPT0)
{
        if (dcount > 1)
                {
                        dcount--;
                }
        else if (dcount == 1)
                {
                        out = 0x16;
                        pcount = 0x14;
                        dcount = 0x00;
                        PORTC = out;
                }
        else if (pcount > 1)
                {
                        pcount--;

                        if (out == 0x16)
                                {
                                        out = 0x19;
                                }
                        else
                                {
                                        out = 0x16;
                                }

                        PORTC = out;
                }
        else if (pcount == 1)
                {
                        out = 0x15;
                        pcount = 0x00;
                        PORTC = out;
                }
        else if (pcount == 0)
                {
                        out = 0x00;
                        dcount = 0xBB8;
                        PORTC = out;
                }
}
```
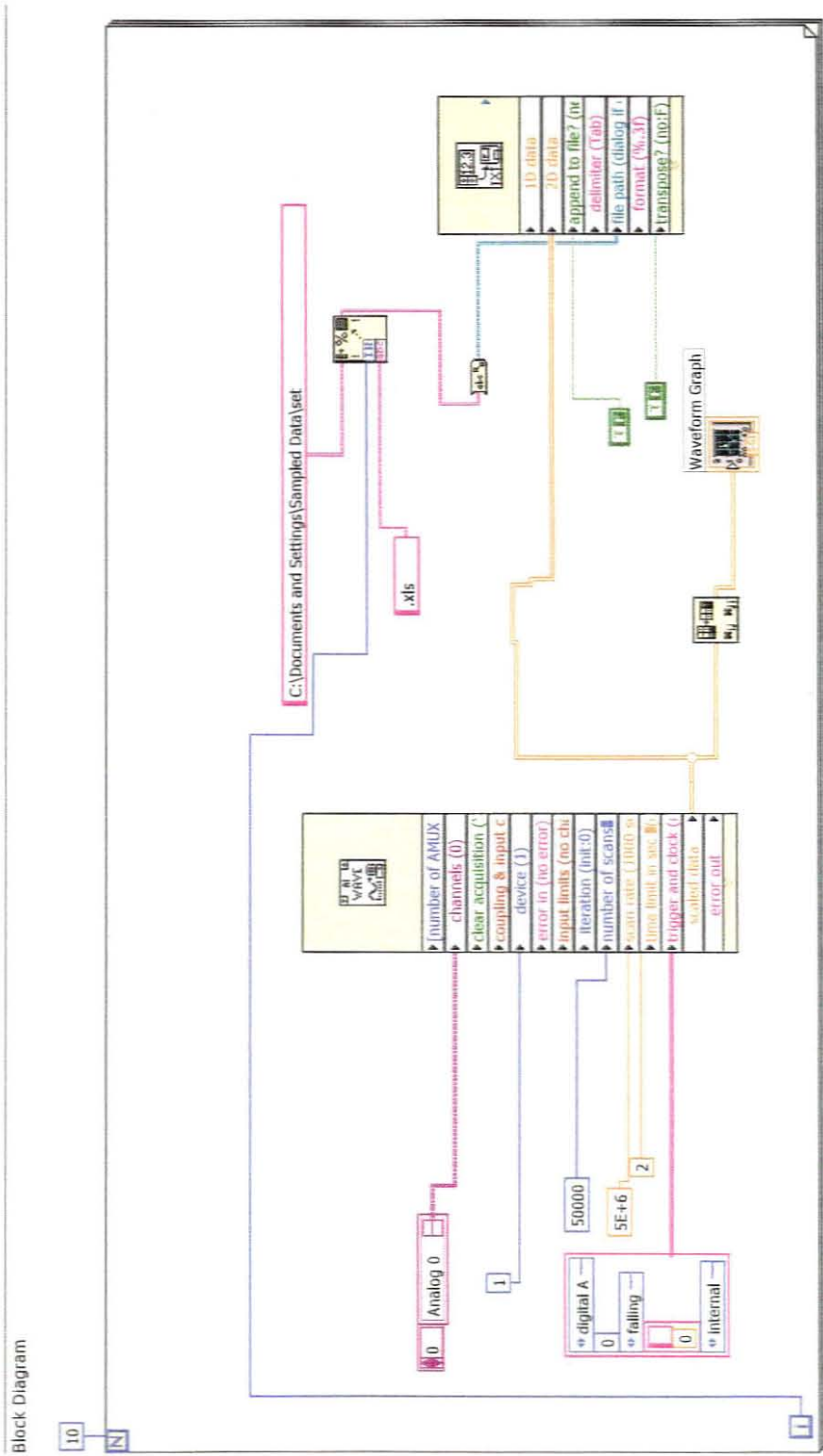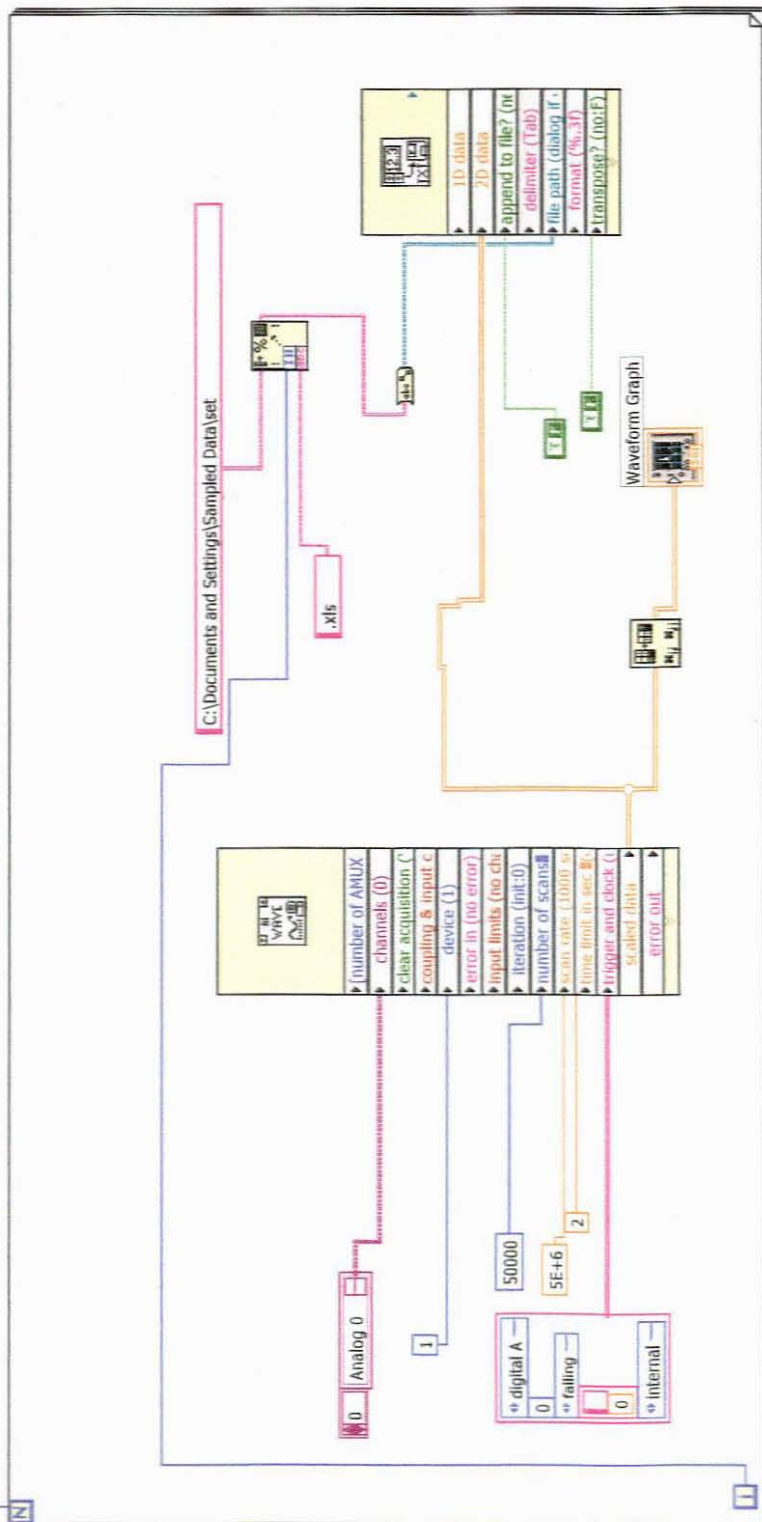
Appendix C

NI Labview Visual Interface

Figure C.1: The block diagram of the Labview Visual Interface used to sample the recovered echo pulses to a file for processing purposes.

Figure C.1: The block diagram of the Labview Visual Interface used to sample the recovered echo pulses to a file for processing purposes.